Contrib Mineral Petrol (2005) 149: 57–84
DOI 10.1007/s00410-004-0635-6

ORIGINAL PAPER

Nigel M. Kelly · Simon L. Harley

An integrated microtextural and chemical approach to zircon geochronology: refining the Archaean history of the Napier Complex, east Antarctica

Received: 16 March 2004 / Accepted: 20 October 2004 / Published online: 9 February 2005

Abstract Integrated textural and chemical characterisation of zircon is used to refine the U–Pb geochronology of the Archaean, ultra-high temperature Napier Complex, east Antarctica. Scanning electron microscope characterisation of zircon and the rare earth element compositions of zircon, garnet and orthopyroxene are integrated to place zircon growth in an assemblage context, thereby providing tighter constraints on the timing of magmatic and metamorphic events. Data indicate that magmatism occurred in the central and northern Napier Complex at ca. 2,990 Ma. A regional, relatively low-pressure metamorphic event occurred at ca. 2,850–2,840 Ma. Mineral REE data from garnet-bearing orthogneiss indicate that ca. 2,490–2,485 Ma U–Pb zircon ages provide an absolute minimum age for the ultrahigh temperature (UHT) foliation preserved in this rock. Internal zircon zoning relationships and estimated zircon-garnet D_{REE} values from paragneiss suggest that an absolute minimum age of ultra-high temperature metamorphism is ca. 2,510 Ma, but that it is more likely to be older than ca. 2,545 Ma. We suggest that the high proportion of published zircon U–Pb data with ages between ca. 2,490–2,450 Ma reflects late, post-peak zircon growth and does not date the timing of *peak* UHT metamorphism.

Electronic Supplementary Material Supplementary material is available for this article at http://dx.doi.org/10.1007/s00410-004-0635-6

Editorial Responsibility: I. Parsons

N. M. Kelly (✉) · S. L. Harley
Grant Institute of Earth Science, School of Geosciences,
University of Edinburgh, Kings Buildings,
West Mains Rd, Edinburgh, EH9 3JW, UK
E-mail: nigel.kelly@glg.ed.ac.uk
Tel.: +44-131-6505885
Fax: +44-131-6683184

Introduction

In-situ ion microprobe analysis of zircon is generally the method of choice for obtaining U–Pb ages for poly-metamorphic rocks. However, despite its utility and widespread application this approach can be biased. The ages we retrieve are commonly dependent on the parts of individual zircon grains we choose to analyse, and hence are heavily dependent our interpretation of internal zircon textural patterns. The increased use of cathodoluminescence (CL) and backscattered electron (BSE) image analysis has allowed more focussed targeting of particular zones within individual zircon grains and interpretation of data populations based on more than a statistical approach. Moreover, the use of scanning electron microscope (SEM) imaging has led to attempts to link zoning patterns or textures in zircon grains to igneous or metamorphic origins (Pupin 1980; Vavra 1990; Hanchar and Miller 1993; Hanchar and Rudnick 1995; Watson and Liang 1995; Vavra et al. 1996; Mezger and Krogstad 1997; Rubatto et al. 1998; Schaltegger et al. 1999; Hoskin and Black 2000; Rubatto and Gebauer 2000). For example, it is now widely recognised that fine-scaled oscillatory zoning in zircon reflects growth from a (felsic) magma (Vavra 1990, 1994; Vavra et al. 1996; Mezger and Krogstad 1997; Rubatto and Gebauer 2000). However, interpretation of internal zoning textures and ages of zircon thought to have formed during metamorphism is more ambiguous.

The origin of particular metamorphic zircon textures that have formed by growth of new zircon or recrystallisation of existing zircon is not always entirely clear (e.g., Schaltegger et al. 1999; Kelly et al. 2002). Moreover, the relative timing of growth or recrystallisation of zircon with respect to prograde, peak or retrograde metamorphism is seldom considered in most geochronological studies. It is possible in some circumstances to relate texturally the sub-solidus growth of zircon to the breakdown of particular minerals during retrograde metamorphism of metapelitic rocks (Fraser et al. 1997;

Pan 1997; Degeling et al. 2001), although this is more difficult in rocks with assemblages that are less reactive. As the age of metamorphic zircon is commonly used along with other techniques to define the duration of metamorphic events and thereby place constraints on crustal processes (Hawkins and Bowring 1999; Hermann et al. 2001; Boger et al. 2002), resolving the relative timing problem is essential.

This contribution reports a potentially powerful means of linking zircon growth/recrystallisation to metamorphic events by using an integrated SEM imaging and trace/rare earth element chemical approach. This technique as applied to zircon grains and associated major minerals, is used to aid the interpretation of U–Pb zircon data from four samples from the Archaean Napier Complex. These samples were selected from a suite dated by Harley and Black (1997) in which analyses were guided by petrological microscope alone and without the aid of CL or BSE imaging techniques. Initial CL and BSE inspection of the original SHRIMP analysis pits with respect to internal zoning patterns revealed that these analyses preferentially targeted core zones so that the significance of zircon outer zones and rims could not be properly evaluated. Moreover, Harley and Black (1997) were not able to distinguish magmatic from metamorphic zircon. In the present study we have used detailed CL and BSE images and REE chemistry to reinterpret the original U–Pb age data presented by Harley and Black (1997), and to guide further SHRIMP analysis. REE patterns have been used to link zircon generations with the growth or presence of major silicate minerals, and thereby place the zircon within an assemblage context. The combined REE and age data have been used to revise and refine aspects of the extended history of the Napier Complex during the middle to late Archaean. As a terrane that preserves regionally extensive occurrences of ultrahigh temperature (UHT) metamorphic assemblages, the ability to refine the chronology and duration of metamorphic events in the Napier Complex has important implications for understanding processes that operate in the deep continental crust.

Geological setting

The Napier Complex is an Archaean cratonic block that comprises the coastal outcrops and islands, and inland mountain ranges of Enderby Land between 48°E–57°E and 66°S–68°S, in the East Antarctic Shield (Fig. 1). The Complex contains some of the oldest exposed rocks on Earth, with igneous precursors to orthogneisses as old as ca. 3,800 Ma (Black et al. 1986a; Harley and Black 1997), and preserves evidence for some of the highest grades of metamorphism recorded in the continental crust (Harley 1998; Harley and Motoyoshi 2000). Three major episodes of deformation affected the terrane between ca. 2,990 and 2,450 Ma, after which this terrane remained essentially undeformed, except for reworking of its eastern and western margins (Sandiford and Wilson 1984; Sheraton et al. 1987; Shiraishi et al. 1997; Kelly et al. 2000).

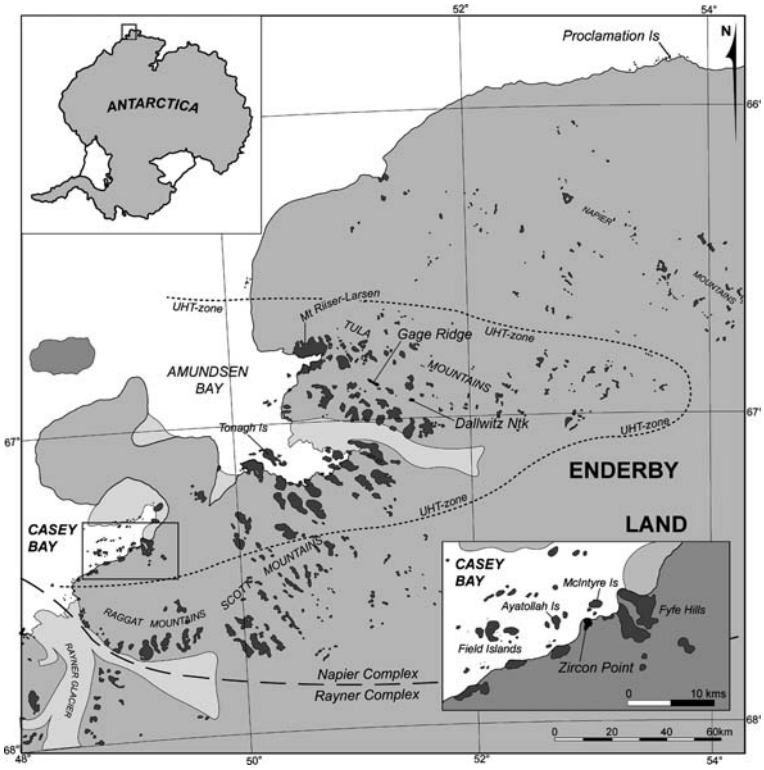

Fig. 1 Outcrop map of the western Napier Complex, Enderby Land, east Antarctica. Areas of outcrop are indicated in dark grey. Samples locations (Gage Ridge, Dallwitz Nunatak, Proclamation Island, Zircon Point) are in-filled black and labelled. The approximate extent of UHT mineral assemblages (UHT-zone) is indicated by the short dashed line (after Harley and Motoyoshi 2000), and the south-western boundary between the Napier and Rayner Complexes is indicated by the long dashed line (after Sheraton et al. 1987). *Inset*: close-up of the Casey Bay region and location of Zircon Point

The Napier Complex is dominated by ca. 2,990–2,800 Ma tonalitic to granitic orthogneiss (Black et al. 1986b; Sheraton et al. 1987; Harley and Black 1997; Hokada et al. 2003), with locally extensive occurrences of layered metasediments, and minor mafic and ultramafic units (Sheraton et al. 1987). The terrane has been affected by at least three deformation events (James and Black 1981; Sandiford and Wilson 1984; Sheraton et al. 1987) some of which have not been recognised throughout the complex (Harley and Black 1997). D_1 resulted in the development of a regionally extensive flat-lying and intensely lineated S_1 gneissosity. Compositional layering is folded by recumbent F_1 folds that are up to tens of metres in amplitude, with deformation causing the transposition and interleaving of units. D_2 refolded S_1 about tight F_2 folds that have recumbent to reclined axial planes. An S_2 gneissosity was only developed locally. Regional dome and basin structures developed during D_3 through broad upright folding of earlier layering and structures. S_3 fabrics are typically developed only locally in F_3 hinges, but in some areas D_3 was intense enough to produce a pervasive fabric. The high-grade fabrics are cut by three generations of dykes (metatholeiite: ca. 2,400 Ma; high-Mg mafic dykes: ca. 2,350 Ma; and the tholeiitic Amundsen Dykes: ca. 1,200 Ma; Sheraton et al. 1987), which pre-date the formation of amphibolite facies shear and pseudotachylite zones (D_4–D_5; Harley 1985; Sandiford 1985). This late deformation may be attributed to Rayner (ca. 1,000–900 Ma) and/or Pan African (ca. 550–500 Ma) aged reworking (Sandiford 1985; Shiraishi et al. 1997) and fluid infiltration (498 ± 1.7 Ma, Carson et al. 2002a). Late lamproite dykes (482 ± 3 Ma) also intrude the complex.

The Napier Complex is characterised by the regional occurrence of UHT mineral assemblages that imply that peak metamorphic conditions of $T \approx 1{,}050$–$1{,}120$°C and $P \approx 7$–11 kbars accompanied D_1–D_2 (Dallwitz 1968; Ellis et al. 1980; Grew 1980, 1982; Sheraton et al. 1980, 1987; Harley 1985, 1998; Sandiford 1985; Motoyoshi and Hensen 1989; Hensen and Motoyoshi 1992; Harley 1998; Hokada et al. 1999; Harley and Motoyoshi 2000). Extreme temperatures were restricted to a central zone (marked on Fig. 1) with slightly lower temperatures recorded outside of this area. UHT metamorphism in the Napier Complex was followed by a period of near-isobaric cooling (IBC), which occurred at pressures of less than 8 kbar in the northern parts of the Complex (Amundsen Bay and Tula Mountains) and at pressures of 9–10 kbar in areas further south (Scott Mountains: Sheraton et al. 1980, 1987; Ellis and Green 1985; Harley 1985, 1998; Harley and Hensen 1990; Hensen and Motoyoshi 1992; Harley 1998; Osanai et al. 1999). Hollis and Harley (2002) reported evidence for apparent-isothermal decompression through 1–3 kbar at temperatures of greater than 1,000°C, prior to IBC in the UHT region.

The ages of deformation events and of the UHT and other metamorphic events have been the subject of considerable debate. Using ages from syn-metamorphic charnockitic pegmatites, Grew and Manton (1979) suggested that high-temperature metamorphism (later to be characterised as UHT, and linked to the D_2 event by Grew et al. 1982) occurred in the Napier Complex at ca. 2,500 Ma. A Rb/Sr isochron and zircon ages of ca. $3{,}100 \pm 500$ Ma from paragneiss were interpreted by Black and James (1979) to reflect the timing of the high-grade D_2 event. This was later reinforced by James and Black (1981) using zircon upper intercept ages of ca. 3,050 Ma. James and Black (1981) further suggested that those zircon ages that clustered near ca. 2,500 Ma reflected resetting associated with D_3 retrograde (but still amphibolite to granulite facies) metamorphism.

An older age for D_1 was again suggested on the basis of a Rb/Sr whole rock isochron age of $3{,}072 \pm 34$ Ma from a "syn-D_1" charnockite at Proclamation Island (Black et al. 1986b). This sample was subsequently re-dated using U/Pb SHRIMP techniques, producing an age of $2{,}980 \pm 9$ Ma (Harley and Black 1997), but as the sample came from outside the region of extreme metamorphism the age was not considered an estimate for the UHT event. The timing of D_2 at 2,840 $+220/-280$ Ma (Rb/Sr whole rock isochron age; Black et al. 1986b) was initially based on the age of a "syn-D_2" granite body from the Napier Mountains. However, U/Pb zircon ages inferred to reflect crystallisation of "syn-D_1" orthogneiss at Dallwitz Nunatak led Harley and Black (1997) to suggest that D_1 could be no older than ca. 2,850 Ma and that D_1–D_2 and UHT metamorphism occurred within the period ca. 2,850–2,820 Ma. Within this context, the timing of D_3 was inferred by these and other authors to have occurred between ca. 2,480 and 2,450 Ma (James and Black 1981; Black et al. 1983b, 1986a, 1986b; Harley and Black 1997).

The abundance of metamorphic zircon with ages between 2,500 and 2,450 Ma (Black et al. 1983a, 1983b, 1986a, 1986b; McCulloch and Black 1984; Harley and Black 1997; Shiraishi et al. 1997; Grew et al. 2001; Asami et al. 2002; Carson et al. 2002b; Crowe et al. 2002; Hokada et al. 2003, 2004) supported the original interpretations of Grew and Manton (1979) and Grew et al. (1982) that widespread high-grade metamorphism occurred closer to this younger age. Moreover, "syn-tectonic" ca. 2,456 Ma pegmatites in Casey Bay interpreted to be "syn-D_3" by Black et al. (1983a) were interpreted by Sandiford and Wilson (1984) to have intruded during syn-D_2 boundinage, and were suggested by Grew (1998) to preserve UHT assemblages. It is now accepted by most, if not all workers in the Napier Complex, that pre-2,800 Ma ages reflect earlier magmatism and metamorphism that are unrelated to the UHT event. However, the precise timing of peak metamorphism, and the duration of the UHT event is still a matter for debate. Orthopyroxene-bearing felsic orthogneiss interpreted to have been intruded at ca. 2,626 Ma and prior to the development of a UHT S_1 fabric (Carson et al. 2002b) places an upper limit on UHT metamorphism, whilst zircon data from a leucosome that cuts

UHT fabrics at McIntyre Island (Harley et al. 2001; Harley 2002) suggests that the UHT event occurred between ca. 2,590 and 2,550 Ma. Multiple populations of metamorphic zircon in Tonagh Island orthogneiss (e.g., minor growth at 2,546 ± 13 Ma, abundant growth at 2,477 ± 9 Ma: Carson et al. 2002b) reveal the potential complexity in zircon forming episodes during this event. Resolving these problems in interpreting the U–Pb age data is not only important for the "local" Napier Complex history but also more generally for informing the debate on the responses of zircon to HT/UHT metamorphism in the deep continental crust.

Sample descriptions

The four samples selected from Harley and Black (1997) are massive granitic orthogneiss from Gage Ridge (78285013; Tula Mountains, Fig. 1); charnockitic orthogneiss from Proclamation Island (80285045; northern Napier Complex); granitic orthogneiss from Dallwitz Nunatak (78285005; Tula Mountains); and paragneiss from Zircon Point (80285037; Casey Bay).

The *Gage Ridge orthogneiss* is composed of granoblastic mesoperthite and quartz. Scattered trails of orthopyroxene (~0.5%) define a coarse gneissosity. The *Proclamation Island charnockite* is interpreted to have intruded during a "local" D_1–M_1 event (Black et al. 1986b; Harley and Black 1997) and is composed of coarse-grained perthite, quartz, plagioclase and orthopyroxene, with accessory zircon and opaque minerals. Secondary hornblende occurs as narrow (< 0.25 mm) rims on the opaque minerals. Accessory clinopyroxene and apatite were also reported by Harley and Black (1997), although not identified in the samples studied here. The lack of mesoperthite suggests that this rock was recrystallised at lower temperature compared with the UHT conditions recorded in the Tula-Scott Mountains regions. The *Dallwitz Nunatak orthogneiss* is composed of granoblastic mesoperthite, quartz, orthopyroxene and minor garnet (not previously reported). Trails of scattered orthopyroxene define coarse gneissosity. The orthogneiss was interpreted to have intruded "syn-D_1". The *Zircon Point paragneiss* is composed of porphyroblastic garnet in a quartz-feldspar (including mesoperthite) matrix. A coarse-grained gneissosity is defined by alternating bands of garnet-present and -absent material and by elongate garnet porphyroblasts.

Zircon characterisation

Analytical methods

Zircon grains from standard epoxy grain mounts and thin sections from all four samples were imaged in detail using the Phillips XL30 SEM located at the Grant Institute of Earth Science, University of Edinburgh. CL images were obtained at 15 kV and ~30 μA and BSE images were obtained at 20 kV and 40–50 μA. SIMS analysis of zircon, garnet, orthopyroxene and amphibole was carried out at the NERC Ion Microprobe Facility, University of Edinburgh, using a Cameca ims-4f ion microprobe. Analytical and correction procedures follow those outlined by Hinton and Upton (1991). Minerals were analysed using a 14.5 keV primary beam of O^- at ~5 nA primary current focussed to a 15–20 μm spot, with secondary ions measured at 120 V offset (zircon) and 75 V offset (garnet, orthopyroxene, amphibole). For each analysis ten cycles were made through the masses of interest. Ion yields were calculated using the NIST SRM-610 glass standard and concentrations were referenced against Si, as determined by electron microprobe (Suppl. data). For zircon, corrections were made for $ZrSiO^+$ overlap on $^{138}Ba^+$, $^{139}La^+$, $^{140}Ce^+$ and $^{141}Pr^+$ using count rates measured at mass 134. Analytical reproducibility during and between analytical periods was tested using analyses of the 91500, SL1 and SL13 zircon standards (zircon analysis) and "ddigrt" standard (garnet and orthopyroxene analysis). REE data are summarised in Table 1, whilst full ion microprobe data can be found in Supplementary Data Tables 1, 2 and 3.

Zircon textural and REE features

The relative abundance of the light rare earth elements (LREE: La–Sm) to middle (MREE: Gd–Dy) and heavy rare earth elements (HREE: Ho–Lu) in zircon has been demonstrated to vary according to the environment in which the zircon forms or is modified (Bea et al. 1997; Bea and Montero 1999; Rubatto et al. 2001; Rubatto 2002; Whitehouse and Kamber 2003). For example, igneous zircon is commonly characterised by a steeply positive, chondrite-normalised La–Lu compositional pattern (e.g., Fig. 2), due to a preference for the smaller ionic radius HREE over larger ionic radius LREE (Murali et al. 1983; Heaman et al. 1990; Hinton and Upton 1991; Barbey et al. 1995; Hoskin and Ireland 2000; Whitehouse and Kamber 2002, 2003). However, zircon formed or modified during metamorphism may deviate from this pattern (e.g., Rubatto 2002; Whitehouse and Platt 2003). Although zircon grown from or in the presence of anatectic melt may be considered by some authors to be "igneous" by definition (e.g., Hoskin and Black 2000), the resulting REE pattern will deviate from typical igneous patterns on the basis of the melt composition and volume (Whitehouse and Kamber 2003). The composition of zircon that forms through subsolidus growth will be affected by concurrent growth or resorption of other minerals such as garnet, which sequesters HREE, or monazite, which sequesters LREE (Schaltegger et al. 1999; Bea and Montero 1999; Rubatto et al. 2001; Hermann et al. 2001; Rubatto 2002; Whitehouse and Platt 2003). Hence the variation in relative concentration of the REE in zircon provides a powerful tool with which to interpret the textural and

Table 1 Summary of average SIMS values for key trace element data and REE indicator ratios for each zircon type

	Th/U	Hf (ppm)	Y (ppm)	P (ppm)	$Yb/Dy_{(n)}$	$Yb/Gd_{(n)}$	Eu/Eu*	Ce/Ce*
Gage ridge orthogneiss								
Magmatic cores	0.37 (0.05–0.08)	12541 (9600–15500)	1685 (943–2220)	519 (286–789)	4.6 (4.0–4.9)	19.5 (10.6–28.8)	2.9 (1.9–4.1)	35.3 (11–92)
Altered magmatic	0.11 (0.05–0.08)	19391 (14300–26300)	1782 (676–3307)	924 (446–1265)	5.0 (2.9–6.6)	35.4 (13.7–61.1)	5.9 (7.0–9.2)	19.3 (8–34)
Low CL cores/rims 1	0.06 (0.05–0.06)	15848 (14700–17600	1051 (701–1488)	669 (462–1013)	5.2 (2.8–6.7)	30.9 (11.6–41.0)	9.2 (4.6–17.7)	19.2 (5–29)
Low CL cores/rims 2	0.18 (0.13–0.29)	15268 (13700–16800)	811 (717–922)	635 (552–757)	2.1 (1.6–2.3)	6.1 (4.5–9.0)	8.3 (3.5–12.0)	14.3 (4–27)
Low CL core	0.07	22118	520	312	0.5	1.1	9.3	48.5
Proclamation Is. charnockite								
Magmatic cores	0.47 (0.42–0.54)	13124 (11200–14000)	1307 (784–2320)	555 (405–803)	4.9 (4.4–7.4)	20.5 (18–24)	0.06 (0.01–0.12)	34.0 (31–38)
Altered magmatic	0.22 (0.14–0.43)	15045 (13200–17300)	749 (444–1154)	329 (242–523)	7.9 (5.0–9.2)	41.1 (21–49)	0.12 (0.05–0.23)	40.7 (12–84)
Low CL overgrowths	0.32 (0.02–0.38)	14091 (13500–14800)	1013 (653–1206)	457 (404–498)	5.7 (5.1–6.8)	26.6 (22–34)	0.04 (0.04)	80.6 (66–105)
High CL rims	0.89 (0.50–1.80)	15225 (13300–16400)	748 (524–1079)	390 (319–514)	6.1 (5.5–6.7)	30.8 (28–39)	0.05 (0.04–0.06)	46.9 (15–108)
Dallwitz Ntk orthogneiss								
Magmatic cores	0.61 (0.30–0.94)	12349 (11000–14500)	1175 (341–2466)	675 (254–917)	4.0 (3.6–4.5)	12.6 (9–16)	0.3 (0.1–0.4)	14.8 (4–30)
Low CL rims	0.04 (0.03–0.08)	20752 (18200–22400)	1027 (874–1768)	870 (609–1188)	8.9 (4.6–10.6)	67.3 (48–90)	0.1 (0.05–0.2)	4.5 (2–9)
Planar and sector zoned grains	0.15 (0.11–0.22)	17125 (16000–19500)	499 (225–655)	475 (298–607)	1.0 (0.6–1.2)	2.0 (0.8–3)	0.02 (0.01–0.04)	11.9 (7–17)
Zircon Point paragneiss								
Magmatic cores	0.36 (0.33–0.41)	12587 (11300–13400)	1281 (703–2160)	637 (364–1038)	4.5 (4.1–5.0)	17.1 (10.5–23.2)	0.2 (0.1–0.5)	18.5 (4–34)
Altered zircon/embayments	0.4 (0.3–0.6)	15982 (15300–16500)	310 (204–1331)	373 (267–429)	1.4 (0.9–2.2)	1.6 (1.0–2.5)	0.1 (0.1–0.2)	24.7 (7–38)
Low-mod CL grains	0.33 (0.23–0.46)	16572 (15700–13400)	658 (194–315)	538 (326–756)	0.6 (0.5–0.7)	0.6 (0.5–0.8)	0.1 (0.1–0.2)	33.1 (12–38)
Mod CL rims	0.26 (0.24–0.28)	16853 (16700–16900)	254 (194–315)	336 (321–351)	0.7 (0.6–0.7)	0.7 (0.7–0.8)	0.2 (0.1–0.2)	29.2 (23–36)
High CL outer cores/rims	1.21 (0.65–1.38)	15926 (14300–17100)	250 (208–299)	486 (364–581)	0.9 (0.7–1.2)	1.0 (0.7–1.4)	0.1 (0.05–0.1)	15.1 (2–28)
Low CL rims	0.17 (0.04–0.31)	16248 (15200–17300)	282 (253–312)	522 (357–687)	0.8 (0.7–0.8)	0.8 (0.7–0.9)	0.2 (0.1–0.4)	12.2 (3–21)

Values in parentheses (right side of each data column) are the data range from which average values (left) were calculated. The value for the Gage Ridge Orthogneiss "weakly luminescent core" reflects a single data point; Th/U ratios are from SIMS data and not SHRIMP analyses.

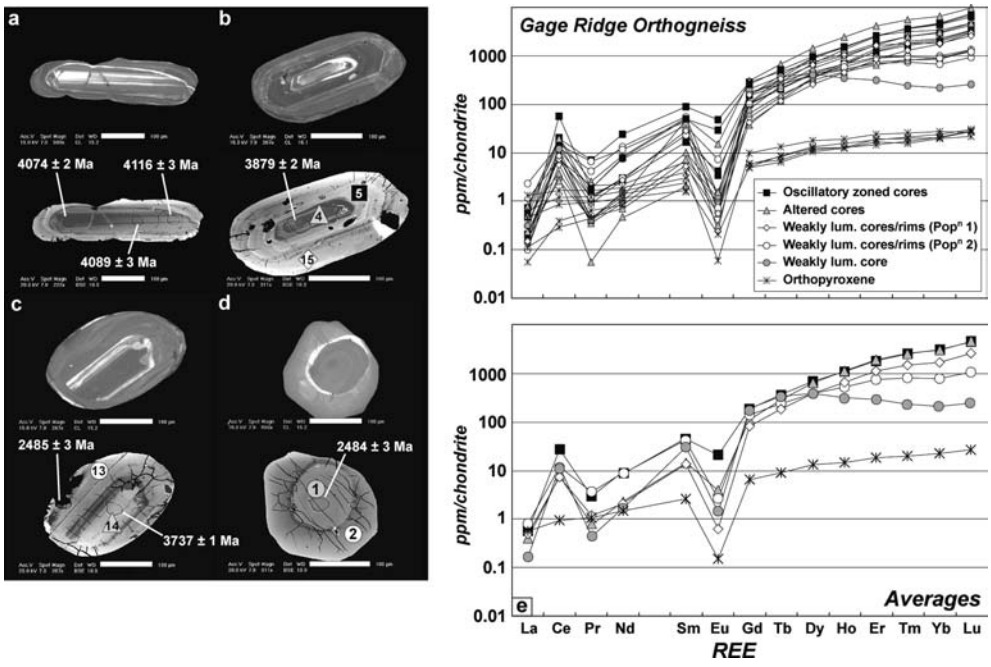

Fig. 2 Representative SEM images (Cathodoluminescent—CL, and Backscattered Electron—BSE) and REE data for zircon grains from Gage Ridge Orthogneiss. All scale bars are 100 μm. **a** CL (top) and BSE (bottom) of a zircon with oscillatory zoned (magmatic) core, with weakly luminescent and weakly banded rim. SHRIMP spots are indicated by a white line with corresponding $^{207}Pb/^{206}Pb$ age—errors quoted at 1σ level. Note the healed fractures that cut the core, which have lower luminescence and higher BSE response; **b** Oscillatory zoned (magmatic) core, with weakly luminescent and weakly banded rim. The location of SIMS spots are indicated by numbered symbols matching those for each zircon zoning type in the adjacent REE plots. The numbers correspond to analyses in Supplementary Data Table 1. **c** Zircon grain with a weakly luminescent, altered core surrounded by a patchy-planar banded ca. 2,485 Ma rim; **d** Weakly luminescent, ca. 2,485 Ma core, surrounded by a further weakly luminescent overgrowth of uncertain age. The core is HREE-depleted; **e** Chondrite-normalised "Matsuda" diagrams for REE in zircon and orthopyroxene. Individual values (top) and average values (bottom) are grouped according to zircon zoning pattern, as discussed in the text. Analyses are normalised to the values of Anders and Grevasse (1989)

chemical context of particular zircon generations and therefore their ages.

Gage Ridge (garnet-absent orthogneiss): sample 78285013

Zircon grains from *Gage Ridge orthogneiss* are medium to dark brown in colour and elongate (450×150 μm), stubby or equant (200 μm in diameter) in shape. They are dominated by low to moderately luminescent cores with variably preserved oscillatory zoning, interpreted to be magmatic in origin (Fig. 2a–c). Networks of healed fractures that have lower luminescence may cut zoning (Fig. 2a), or zoning may appear blurred and form a broader banding that is conformable to the general oscillatory geometry (Fig. 2b, c). Oscillatory zoned cores have steep chondrite-normalised REE patterns (average Yb/Gd≈20), typical for igneous zircon (Fig. 2e). In altered zircon, REE patterns are steeper in comparison to the igneous grains (Yb/Gd≈35; although overlap exists between individual analyses), largely driven by depletion in LREE and MREE. This depletion is consistent with preferential expulsion of the larger ionic radii LREE from the zircon during recrystallisation (e.g., Hoskin and Black 2000).

Surrounding these cores, and commonly truncating zoning, are outer cores and rims (Fig. 2a–c) that have low luminescence and may preserve broad concentric banding or be relatively homogeneous. These are interpreted to have formed during sub-solidus metamorphic growth and have been divided into two populations based on REE pattern and age. Population 1 cores and rims generally have lower REE concentrations, but similar La–Lu slopes compared with oscillatory-zoned grains (Yb/Gd≈31). In comparison, Population 2 cores and rims have similar MREE concentrations, but display LREE- and HREE-depleted patterns (Yb/Gd≈6). In addition, a weakly luminescent core (Fig. 2d; filled grey circle in Fig. 2e), is extremely HREE-depleted and approaches a humped, slightly negatively sloping compositional pattern that is typically observed for garnet (Yb/Gd≈1, Yb/Dy≈0.5). Although no garnet has been identified in thin section, the REE pattern of this generation of zircon approaches that seen for zircon that has grown in the presence of garnet, and is distinct from that observed for Population 1. In rare cases, a thin and discontinuous, brightly luminescent outer zircon rim can be observed (Fig. 2c), with similar high CL zircon between oscillatory zoned cores and low CL rims (Fig. 2a).

Orthopyroxene from this sample (X_{Mg} = 0.39–0.41; Al_2O_3 = 1.8–2.1 wt%; see Supplementary Table 4 for full analyses) has a REE depleted profile (MREE–

HREE = 5–30×chondrite), but is only slightly positively sloping (Yb/Gd≈3–4). This is in contrast to an orthopyroxene composition from a purely garnet-absent rock (e.g., Proclamation Island, below) and may indicate growth or equilibration at the same time as or early in the formation of zircon Population 2.

Proclamation Is (garnet-absent charnockite): sample 80285045

Zircon grains from *Proclamation Island charnockite* are euhedral to subhedral, and range in habit from coarse and elongated (450–600×200 μm) to more equant. Oscillatory zoned (magmatic) cores are low to moderately luminescent (Fig. 3a), whilst the inner portions of cores may be broadly homogeneous or weakly banded; banding is conformable to zoning in the outer parts of the core. In some grains fine oscillatory zones may be blurred forming broad diffuse bands (Fig. 3c). Surrounding these oscillatory zoned cores are low to moderately luminescent outer cores and rims that may preserve broad concentric banding (Fig. 3a), or be weakly banded or relatively homogeneous (Fig. 3c). These rims commonly truncate zoning in cores and are thickest at grain terminations (Fig. 3a, c). Rare, weakly luminescent cores with irregular, patchy zoning (Fig. 3b) are inferred to reflect the same generation of zircon. Contrasting with these weakly luminescent zircon cores and rims are moderate to highly luminescent grains that preserve planar growth banding and sector zoning (Fig. 3d), and rims up to 50 μm in width that occur on the weakly luminescent overgrowths (Fig. 3b, c). The mix of broad planar banding, sector and "fir-tree" zoning is typical of zircon that has grown from or in the presence of anatectic melt during high-grade metamorphism (Vavra et al. 1996; Schaltegger et al. 1999; Kelly et al. 2002). All zircon types analysed in this sample have steep chondrite-normalised profiles (Fig. 3e). Altered zircon, and both the weakly and highly luminescent rims are slightly MREE-depleted and hence have slightly steeper REE patterns (averages Yb/Gd≈26–40) compared with oscillatory zoned zircon (Yb/Gd≈20).

Orthopyroxene (X_{Mg} = 0.36–0.39; Al_2O_3 = 0.30–0.42 wt%) has a REE pattern that is slightly steeper than rim and altered zircon, and significantly steeper than orthopyroxene in the Gage Ridge sample (Yb/Gd≈55). Amphibole (X_{Mg} = 0.18–0.25) overgrowths on Fe–Ti oxides are enriched in all REE (> 1,000×chondrite), with a slightly negatively sloping La–Lu pattern and pronounced negative Eu anomaly.

Dallwitz Nunatak (garnet-orthopyroxene-bearing): sample 78285005

In contrast to the previous samples, *Dallwitz Nunatak orthogneiss* contains oscillatory zoned (magmatic) zircon

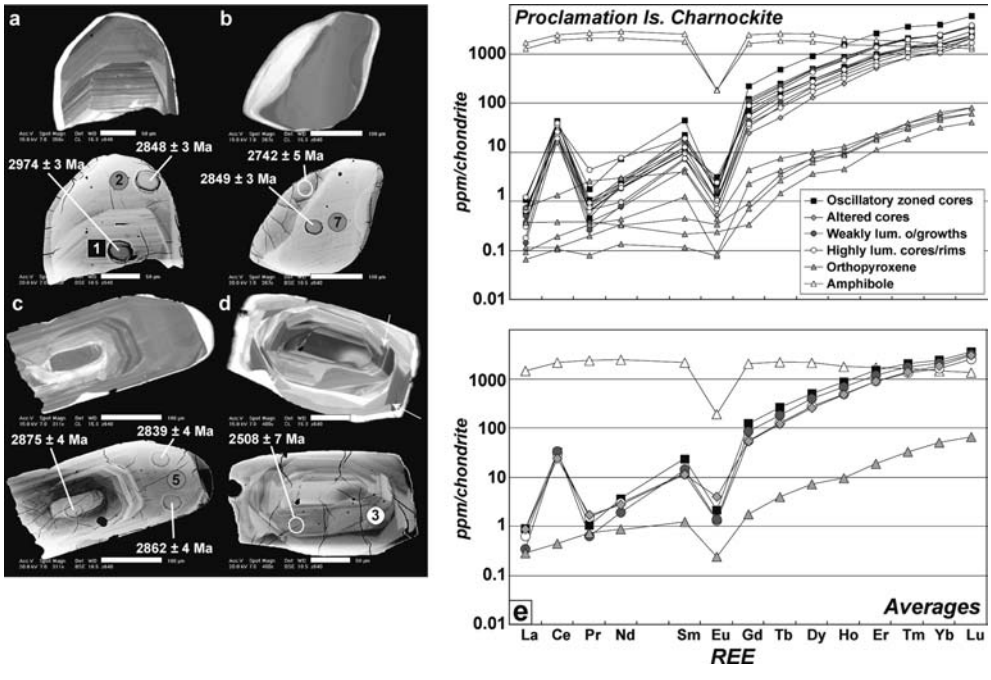

Fig. 3 Representative CL and BSE images and REE data for zircon grains from Proclamation Island charnockite. All ages are $^{207}Pb/^{206}Pb$ ages, with errors quoted at 1σ level. **a** ca. 2,990 Ma oscillatory zoned core surrounded by a ca. 2,850 Ma, banded overgrowth. Note the narrow highly luminescent outer rim. Scale bar is 50 μm. **b** Weakly luminescent, homogeneous core with highly luminescent rim. The age of this rim suggests it formed through partial recrystallisation of pre-existing zircon, not new growth. Scale bar is 100 μm. **c** Altered oscillatory zoned core, with ca. 2,850 Ma weakly banded overgrowth. Scale bar is 100 μm. **d** Moderate to highly luminescent grains with mixed sector zoning and planar growth banding; arrows indicate partially preserved "fir-tree" sector zoning. Scale bar is 50 μm. **e** Chondrite-normalised "Matsuda" diagrams for REE in zircon, orthopyroxene and amphibole

cores that are commonly moderately to highly luminescent (Fig. 4a, d) or more rarely weakly luminescent (Fig. 4c). The zircon cores are mostly elongate (450×150 μm) or stubby in shape and may contain inner regions that are broadly homogeneous but are conformable and gradational into the zoned core regions. Surrounding these cores are weakly luminescent rims, up to 50 μm in width, which preserve planar banding that is broader than the banding seen in oscillatory zoned cores (Fig. 4a, b, d). These rims may be broadly conformable to zoning in cores (Fig. 4a), or truncate and in some cases deeply embay that zoning (Fig. 4d). Rims may also be poorly zoned or homogeneous, with gradation between types in some grains, and may replace sections of cores (e.g. Fig. 4c). Weakly luminescent zircon rims have a distinctly steeper REE profile compared with oscillatory zoned grains, driven by depletion in LREE and MREE, and enrichment in HREE (Yb/Gd≈67 vs 13; Fig. 4f). The LREE-depletion may reflect a crystal-chemical preference in zircon toward the smaller ionic radii REE during metamorphic growth. Alternatively, this pattern may be the result of prior or concurrent growth of LREE-bearing accessory minerals (e.g., monazite), in which case Th would also be depleted relative to U in the zircon. The increased HREE concentration may reflect dissolution and reprecipitation of a more HREE-enriched zircon, or possibly concurrent breakdown of HREE-bearing mineral phases.

Stubby, single growth phase zircon grains that are weakly to moderately luminescent and preserve sector zoning and rare planar growth banding are also observed (Fig. 4e). Rarely, this type of zircon forms rims on oscillatory zoned or sector zoned cores, although is difficult to distinguish from the planar banded rims described above solely from imaging. On the basis of internal zoning, these grains and rims are interpreted to have grown during metamorphism, possibly in the presence of anatectic melt. They are LREE-depleted and have similar MREE concentrations to oscillatory zoned zircon. In contrast to other zircon types, these grains are strongly HREE-depleted (depletion increases with decreasing ionic radii) leading to a flat to slightly positively sloping HREE pattern (Yb/Gd≈2). This is similar to orthopyroxene in this sample (X_{Mg} = 0.35–0.37; Al_2O_3 = 2.2–2.8 wt%), which has a humped, slightly negatively sloping HREE pattern (Fig. 4f; Yb/Gd≈0.9), comparable in shape but not concentration to patterns commonly observed in garnet (Bea et al. 1997; Harley et al. 2001; Rubatto 2002). In addition, orthopyroxene has higher LREE and MREE concentrations compared with other samples by one or two orders of magnitude (LREE–MREE = 20–56×chondrite). Although garnet

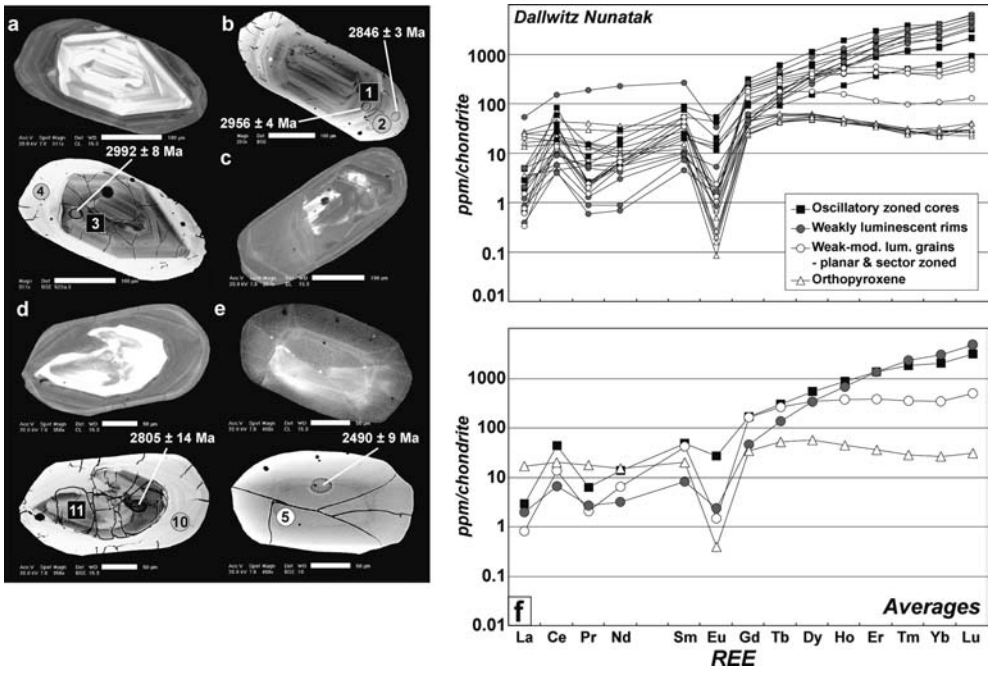

Fig. 4 Representative CL and BSE images and REE data for zircon grains from Dallwitz Nunatak orthogneiss. All ages are $^{207}Pb/^{206}Pb$ ages, with errors quoted at 1σ level. **a** ca. 2,990 Ma oscillatory zircon core surrounded by weakly luminescent, banded ca. 2,850 Ma rim. Scale bar is 100 μm. **b** BSE image of a partially altered oscillatory zoned core (note blurred zoning of the band within which the SHRIMP analysis was taken), with ca. 2,850 Ma, banded rim. Scale bar is 100 μm. **c** CL image illustrating replacement of oscillatory zoned zircon by weakly luminescent and banded zircon. It is not clear if this replacement is via dissolution and re-growth or recrystallisation of the protolith zircon. Scale bar is 100 μm. **d** Oscillatory zoned zircon embayed by weakly luminescent, banded ca. 2,850 Ma, MREE-depleted overgrowth. A band of highly luminescent, altered zircon occurs between the core and overgrowth. Scale bar is 50 μm. **e** ca. 2,490 Ma, weakly luminescent, sector zoned grain. This zircon type is characterised by HREE-depleted compositions. Scale bar is 50 μm. **f** Chondrite-normalised "Matsuda" diagrams for REE in zircon and orthopyroxene. Average values for weakly luminescent zircon rims ignores analysis DN7 due to unfeasibly high LREE, interpreted to reflect partial overlap with a monazite inclusion

could be identified as small fragments in thin section in this sample, these were not suitable for analysis by SIMS. The REE patterns observed in both weakly to moderately luminescent zircon grains and orthopyroxene suggest that they grew or equilibrated during the same metamorphic event, along with the garnet.

Zircon Pt Paragneiss (garnet-bearing): sample 80285037

Zircon Point paragneiss contains large, stubby and equant zircon grains (~200 μm diameter) that commonly contain inherited, oscillatory zoned cores (Fig. 5a) surrounded by extensive overgrowths of "metamorphic" zircon. Oscillatory zoning in some grains may be blurred (Fig. 5b) or intensely disrupted (Fig. 5c). "Metamorphic" zircon can be divided into four broad textural types that, in contrast to inherited oscillatory zoned zircon cores (Yb/Gd≈17), have flat, HREE(+Y)-depleted and slightly negatively sloping MREE–HREE profiles (Fig. 5f; Yb/Gd≈0.6–1.0), indicative of zircon that has grown in the presence of garnet (Harley et al. 2001; Whitehouse and Platt 2003).

Population 1 comprises large (~200 μm) equant grains that are moderately luminescent and preserve planar growth banding and sector zoning (Fig. 5d). Population 2 has moderately luminescent rims (typically 10–25 μm, but up to 50 μm thick) that are planar growth banded and commonly form on oscillatory zoned cores (Fig. 5b, c). Population 3 has highly luminescent outer cores and rims that commonly form extensive overgrowths and exhibit mixed planar growth banding, sector and "fir-tree" zoning (Fig. 5a, e). The zoning patterns from Populations 2 and 3 are characteristic of zircon that has grown from or in the presence of anatectic melt at high metamorphic grades. Population 4 comprises very weakly luminescent, discontinuous rims on highly luminescent zircon (3), and is not well represented among the grains studied. Population 1 zircon grains have the highest concentration of MREE–HREE (200–530×chondrite), while texturally younger overgrowths (Populations 2–4) have lower MREE–HREE concentrations (80–250×chondrite).

Many inherited magmatic grains from the Zircon Point sample have been affected by varying degrees of recrystallisation/alteration or annealing. Minor cases include blurring of zoning at the intersection between crystal faces producing zones of higher luminescence (Fig. 5b). However, more extreme disturbance of oscillatory zoning is manifested as "convoluted" zoning (Fig. 5c; after Hoskin and Black 2000), where zones can be traced into curved and distorted patterns. Disturbed zones are slightly depleted in La and Pr, whilst the MREE show a range similar to that observed for magmatic zircon. However, the HREE may show a variation in concentration between grains, from steep profiles (Yb/Gd≈31) similar to pristine

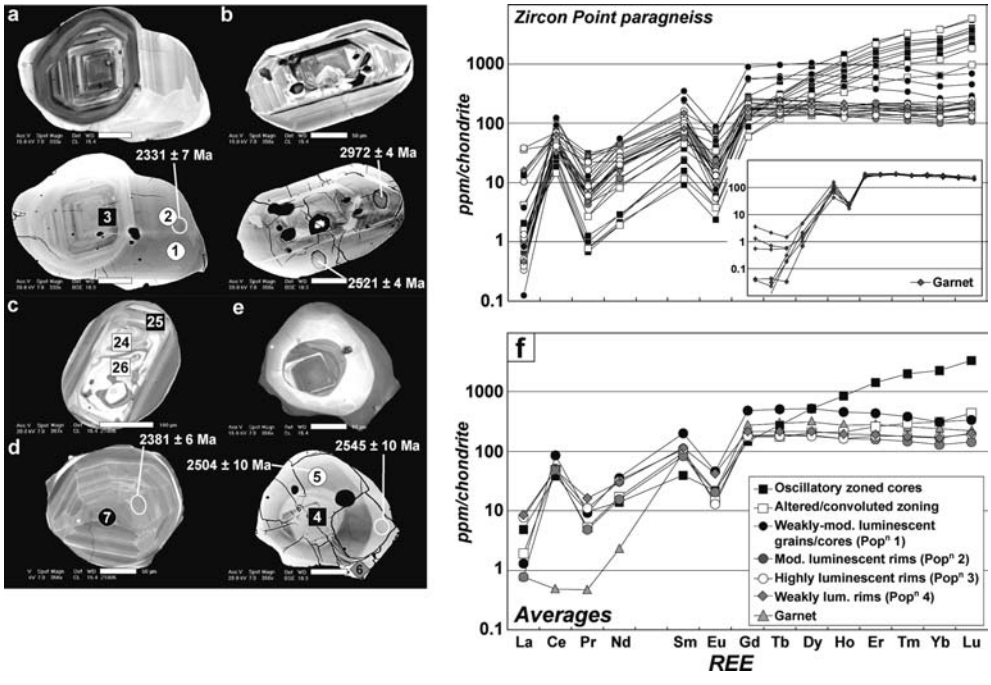

Fig. 5 Representative CL and BSE images and REE data for zircon grains from Zircon Point paragneiss. All ages are $^{207}Pb/^{206}Pb$ ages, with errors quoted at 1σ level. **a** Inherited magmatic core surrounded by thick overgrowth of highly luminescent "Population 3" zircon. Scale bar is 50 μm. **b** Inherited magmatic core with moderately luminescent, planar banded rims (Population 2). Note the extensive alteration within the inner core. Scale bar is 50 μm. **c** Intensely altered inherited zircon with convoluted zoning patterns. The grain is rimmed by planar banded "Population 2" zircon. Scale bar is 100 μm. **d** Moderately luminescent, planar banded and sector zoned grain (Population 1). Scale bar is 50 μm. **e** Three phase zircon grain with inherited, magmatic core, highly luminescent "Population 3" overgrowth and an outer rim of weakly luminescent, high U zircon (Population 4). Scale bar is 50 μm. **f** Chondrite-normalised "Matsuda" diagrams for REE in zircon and garnet

igneous zircon compositions, to flat profiles that are similar to newly grown zircon in this sample (see below; Yb/Gd≈1). The latter pattern, in which the HREE are relatively depleted but LREE are not, contrasts with the LREE-depleted patterns observed for recrystallised grains from Gage Ridge orthogneiss and Proclamation Island charnockite, and those reported elsewhere (e.g., Hoskin and Black 2000).

Coarse-grained garnet analysed from the Zircon Point paragneiss ($X_{Pyr} = 0.48–0.50$, $X_{Grs} = 0.02–0.03$) has MREE–HREE profiles that are flat and slightly negatively sloping (Yb/Gd≈0.7; inset Fig. 5f). MREE and HREE concentrations are mid-way between those obtained for weakly to moderately luminescent zircon cores and highly luminescent zircon overgrowths. The concentration of *Y* in garnet is variable (90–400 ppm), as is P (177–450 ppm), and Zr is relatively low (10–93 ppm). No systematic core–rim compositional variations were detected during SIMS or electron microprobe analysis.

Summary

Zircon grains from both orthogneiss and paragneiss samples have a number of common zoning and REE features that allow them to be grouped into two broad growth episodes:

1. Weakly luminescent overgrowths (outer cores and rims) in orthogneiss samples that may be homogeneous or banded, and are interpreted to have formed through sub-solidus growth. These overgrowths have steep, LREE-depleted patterns with rare HREE-enrichment.
2. Weakly, moderately and highly luminescent grains and rims that preserve sector zoning, weak planar banding (Gage Ridge and Dallwitz Nunatak orthogneisses) and strong planar banding (Proclamation Island charnockite and Zircon Point paragneiss). Except for the charnockite, which was sampled outside of the UHT zone, all show minor to major flattening of the HREE without decreases in the LREE. We attribute this to the influence of garnet.

As felsic to intermediate rocks will develop metamorphic garnet at sufficiently high-*P* (and *T*), the distinct REE patterns described above suggest metamorphic growth of zircon in two separate events: an early garnet-absent event inferred to have occurred at low-*P*, followed by a high-*P*/high-*T* event in which garnet was present only in the UHT zone.

U/Pb SHRIMP geochronology

Analytical procedures followed during the original SHRIMP analytical sessions (Session 1) are covered in detail in Harley and Black (1997), with a summary provided here along with methods used for new data acquisition (Session 2). U/Pb isotope analysis (Sessions 1 and 2) was carried out using the SHRIMP II ion microprobe at the Australian National University (ANU), Canberra, following standard techniques described by Compston et al. (1984) and Williams et al. (1984). Standard zircon SL13, which was embedded in the grain mount during Session 1 ($^{206}Pb/^{238}U = 0.0928$, or 572.2 Ma; Claoué-Long et al. 1995) was removed following analysis. New fragments of SL13 and FC1 standard zircon ($^{206}Pb/^{238}U = 0.1859$, or 1,099.1 Ma; Paces and Miller 1993) were mounted prior to Session 2. U/Pb isotopic data from session 2 were reduced by C.M. Fanning (ANU) according to the methods covered in detail by Williams (1998), and using the computer program Squid 1.03 (Ludwig 2001). The Pb/U ratios were normalised relative to $^{206}Pb/^{238}U$ ratio of the FC1 standard, with U concentrations referenced against the SL13 standard. Corrections for common Pb were made using the measured $^{204}Pb/^{206}Pb$ ratio. Uncertainties quoted in Tables 2, 3, 4 and 5 and in the text for *individual analyses* (ratios and ages) are at the 1σ level. All uncertainties in calculated *group* ages are reported at 95% confidence limits; plots and age calculations have been made using the computer program ISOPLOT/EX v2.49 (Ludwig 1999).

Gage Ridge orthogneiss: sample 78285013

No new SHRIMP data were collected from the Gage Ridge sample. However, the existing data were reinterpreted with the benefit of CL and BSE images. U/Pb isotopic data are scattered along concordia (Fig. 6a), with a number of the data significantly discordant (up to 13%), suggesting a degree of isotopic mobility. Reverse discordance in some of the oldest data is interpreted to reflect isotopic Pb migration and preferential incorporation into the areas of the zircon analysed (Harley and Black 1997). An alternative explanation (Wiedenbeck 1995) involves higher secondary ion yield of labile Pb in amorphous zircon domains. This is not considered applicable, as there is a pronounced correlation between Pb/U and $^{207}Pb/^{206}Pb$, common Pb contents are extremely low ($^{204}Pb/^{206}Pb$ typically < 0.0001) and Zr_2O^+ emission for unknown zircons was the same as interspersed standard zircon (Harley and Black 1997).

Oscillatory zoned cores ($n = 9$), have variable Th/U ratios ranging between 0.05 and 0.7, considered typical for igneous zircon (Fig. 6b, Table 2). Altered grains ($n = 21$) have a similar though slightly wider range of Th/U ratios (0.05–1.1) and commonly preserve remnants of oscillatory zoning. These grains are interpreted to be variably recrystallised igneous zircon and are considered together with unaltered igneous grains for age analysis. The combined data array ($n = 30$) is extremely discordant, defining a Pb-loss line with an upper intercept with the concordia curve at $3{,}851 \pm 62$ Ma (lower intercept = $2{,}740 \pm 110$ Ma; MSWD = 2.2; Fig. 6c), comparable to the age calculated by Harley and Black (1997;

Table 2 Summary of SHRIMP U/Pb zircon results for sample 78285013: Gage Ridge Orthogneiss

Grain. spot	U (ppm)	Th (ppm)	Th/U	$^{204}Pb/^{206}Pb$	Radiogenic ratios						ρ	Age (Ma)				Disc (%)
					$^{206}Pb/^{238}U$	±	$^{207}Pb/^{235}U$	±	$^{207}Pb/^{206}Pb$	±		$^{206}Pb/^{238}U$	±	$^{207}Pb/^{206}Pb$	±	
Oscillatory zoned core																
5.1	477	285	0.60	0.000002	0.92	0.03	57.14	1.69	0.45	0.0008	0.99	4199	123	4089	3	103
5.2	637	440	0.69	0.000015	0.92	0.03	56.75	1.67	0.45	0.0006	0.99	4209	123	4074	2	103
5.3	280	135	0.48	0.000038	0.97	0.03	61.69	1.83	0.46	0.0009	0.99	4381	128	4116	3	106
15.1	1997	106	0.05	0.000028	0.73	0.02	33.04	0.96	0.33	0.0003	1.00	3526	103	3612	1	98
17.1	1899	269	0.14	0.000009	0.57	0.02	18.72	0.55	0.24	0.0003	0.99	2888	84	3121	2	93
18.1	3611	1347	0.37	0.000001	0.79	0.02	38.93	1.13	0.36	0.0002	1.00	3756	109	3737	1	101
19.1	3472	1319	0.38	0.000001	0.86	0.03	45.57	1.33	0.38	0.0002	1.00	4001	116	3848	1	104
22.1	134	51	0.38	0.000017	0.59	0.02	23.20	0.70	0.29	0.0012	0.98	2968	88	3405	7	87
34.1	694	268	0.39	0.000013	0.80	0.02	43.09	1.26	0.39	0.0005	1.00	3778	110	3879	2	97
Disturbed Cores																
1.1	1949	131	0.07	0.000017	0.54	0.02	15.52	0.45	0.21	0.0003	1.00	2775	80	2898	2	96
3.1	3754	254	0.07	0.000040	0.68	0.02	27.76	0.81	0.30	0.0002	0.99	3338	97	3453	1	97
4.1	1068	81	0.08	0.000002	0.58	0.02	19.34	0.57	0.24	0.0004	0.99	2959	86	3124	2	95
6.1	1459	517	0.35	0.000014	0.78	0.02	39.61	1.16	0.37	0.0004	0.99	3728	109	3778	2	99
7.1	1590	260	0.16	0.000011	0.68	0.02	29.91	0.87	0.32	0.0003	1.00	3361	98	3554	2	95
10.1	1711	87	0.05	0.000007	0.52	0.02	13.37	0.39	0.19	0.0002	1.00	2683	78	2723	2	99
12.1	2528	168	0.07	0.000005	0.57	0.02	18.15	0.53	0.23	0.0002	0.99	2899	84	3063	2	95
14.1	3441	326	0.10	0.000008	0.67	0.02	25.99	0.76	0.28	0.0002	0.99	3287	95	3381	1	97
20.1	1635	113	0.07	0.000174	0.57	0.02	18.26	0.53	0.23	0.0003	1.00	2913	85	3065	2	95
21.1	2344	170	0.07	0.000047	0.58	0.02	19.18	0.56	0.24	0.0003	1.00	2940	85	3124	2	94
23.1	2552	546	0.21	0.000006	0.70	0.02	32.29	0.94	0.33	0.0003	1.00	3431	100	3631	1	95
24.1	2244	2288	1.02	0.000003	0.87	0.03	46.54	1.36	0.39	0.0003	0.99	4039	117	3861	1	105
24.2	727	806	1.11	0.000025	0.84	0.02	41.96	1.23	0.36	0.0005	0.99	3944	115	3752	2	105
25.1	3805	1003	0.26	0.000002	0.72	0.03	31.45	0.92	0.32	0.0002	1.00	3500	141	3552	1	99
27.1	289	105	0.36	0.000791	0.74	0.02	34.60	1.03	0.34	0.0011	0.98	3557	104	3666	5	97
28.1	717	205	0.29	0.000032	0.86	0.02	48.23	1.41	0.41	0.0006	0.99	3987	116	3940	2	101
29.1	1591	113	0.07	0.000007	0.57	0.02	18.06	0.53	0.23	0.0003	0.99	2893	84	3061	2	95
30.1	2642	209	0.08	0.000002	0.56	0.02	17.01	0.50	0.22	0.0002	0.99	2871	83	2979	2	96
31.1	1912	154	0.08	0.000004	0.57	0.02	17.46	0.51	0.22	0.0003	0.99	2891	84	3007	2	96
32.1	1649	425	0.26	0.000071	0.56	0.02	17.97	0.53	0.23	0.0003	0.98	2876	83	3064	2	94
33.1	824	45	0.06	0.000111	0.72	0.02	31.33	0.92	0.31	0.0005	0.99	3505	102	3543	2	99
Weakly luminescent outer core/rims																
2.1	2378	204	0.09	0.000019	0.52	0.02	13.96	0.41	0.19	0.0002	0.99	2711	79	2773	2	98
28.2	1294	64	0.05	0.000002	0.53	0.02	13.96	0.41	0.19	0.0003	0.99	2750	80	2744	2	100
9.1	2123	144	0.07	0.000004	0.50	0.01	11.84	0.35	0.17	0.0002	0.98	2592	75	2591	2	100
Planar banded core/rim																
8.1	1721	284	0.17	0.000054	0.49	0.01	10.96	0.32	0.16	0.0002	1.00	2563	75	2484	3	103
13.1	4963	346	0.07	0.000003	0.48	0.01	10.88	0.32	0.16	0.0001	0.99	2547	74	2484	1	103
13.2	2351	415	0.18	0.000024	0.47	0.01	10.60	0.31	0.16	0.0002	1.00	2485	72	2491	2	100
18.2	1265	215	0.17	0.000016	0.45	0.01	10.07	0.30	0.16	0.0003	0.97	2389	69	2485	3	96
Sector zoned/homogeneous cores/rims																
11.1	1968	331	0.17	0.000005	0.47	0.01	10.48	0.31	0.16	0.0002	0.98	2474	72	2480	2	100
16.1	2053	152	0.07	0.000008	0.52	0.02	13.25	0.39	0.18	0.0002	0.98	2702	78	2694	2	100
26.1	1508	76	0.05	–	0.48	0.01	11.49	0.32	0.17	0.0002	1.00	2534	74	2527	3	100

1 Uncertainties given at the one sigma level, *2* Correction for common Pb made using the measured $^{204}Pb/^{206}Pb$ ratio, *3* ρ = error correlation between $^{206}Pb/^{238}U$ and $^{207}Pb/^{235}U$ ratios

3,840 +30/−20 Ma). Analyses of weakly luminescent cores and rims ($n = 10$; Th/U = 0.05–0.18) produce a near to concordant scatter along the concordia curve from 2,773 ± 2 to 2,484 ± 3 Ma (Fig. 6d). Four analyses of Population 2 cores and rims form a concordant cluster at the lower end of the chord, and provide a grouped "concordia age" (after Ludwig 1999) of 2,486 ± 8 Ma (2σ error, MSWD = 0.0056).

Proclamation Island charnockite: sample 80285045

The data from Proclamation Island zircon grains comprise 30 analyses from Sessions 1 and 8 analyses from Session 2 (Fig. 7a). Previous analyses focussed on cores, but included one analysis of a highly luminescent rim. Oscillatory zoned cores ($n = 14$) have only a minor variation in Th/U (0.42–0.65; Fig. 7b, Table 3). One analysis was distinct from the population (18.1), and was rejected from the grouped age calculation. The remaining 13 analyses are slightly discordant and define a chord with an upper intercept with the concordia curve at 2,988 ± 23 Ma (lower intercept = 1,037 ± 630 Ma, MSWD = 3.1; Fig. 7c, inset), within error of the original 2,980 ± 9 Ma ($n = 9$) age (Harley and Black 1997). A further 14 analyses, taken from altered grains, weakly luminescent outer cores and rims with Th/U = 0.2–0.4 scatter along concordia between 2,900 and 2,600 Ma.

Table 3 Summary of SHRIMP U/Pb zircon results for sample 80285045: Proclamation Island Charnockite

Grain. spot	U (ppm)	Th (ppm)	Th/U	Pb* (ppm)	$^{204}Pb/^{206}Pb$	f_{206} (%)	Radiogenic Ratios						ρ	Age (Ma)				Disc (%)
							$^{206}Pb/^{238}U$	±	$^{207}Pb/^{235}U$	±	$^{207}Pb/^{206}Pb$	±		$^{206}Pb/^{238}U$	±	$^{207}Pb/^{206}Pb$	±	
Oscillatory zoned cores																		
2.2	318	145	0.46		0.00006		0.60	0.01	18.18	0.3	0.22	0.0005	0.98	3013	52	2989	4	101
3.1	496	248	0.50		0.00004		0.60	0.01	18.18	0.3	0.22	0.0004	0.98	3036	52	2974	3	102
4.1	348	175	0.50		0.00044		0.59	0.01	17.85	0.3	0.22	0.0005	0.96	2971	51	2988	4	99
5.1	304	157	0.52		0.00019		0.55	0.01	16.51	0.2	0.22	0.0007	0.93	2813	38	2971	5	95
6.1	348	182	0.52		0.00004		0.54	0.01	15.97	0.2	0.21	0.0005	0.97	2798	38	2929	4	96
6.2	287	134	0.47		0.00003		0.57	0.01	17.23	0.3	0.22	0.0006	0.94	2913	40	2971	5	98
6.3	412	201	0.49		0.00002		0.55	0.01	16.50	0.2	0.22	0.0005	0.96	2805	38	2976	3	94
7.1	830	484	0.58		0.00001		0.55	0.01	16.21	0.2	0.21	0.0003	0.98	2830	37	2930	2	97
7.2	881	568	0.65		0.00001		0.55	0.01	16.37	0.2	0.21	0.0003	0.98	2845	37	2936	2	97
9.1	758	384	0.51		0.00001		0.57	0.01	17.22	0.2	0.22	0.0003	0.98	2909	38	2972	2	98
10.1	299	147	0.49		0.00003		0.57	0.01	17.49	0.2	0.22	0.0005	0.97	2902	39	3002	4	97
13.2	261	135	0.52		0.00005		0.55	0.01	16.33	0.2	0.22	0.0005	0.96	2817	38	2951	4	95
14.1	241	119	0.49		0.00009		0.57	0.01	17.50	0.3	0.22	0.0006	0.94	2916	39	2994	4	97
18.1	978	465	0.48		0.00003		0.60	0.01	17.93	0.2	0.22	0.0003	0.98	3042	40	2948	2	103
Altered grains																		
11.1	1473	656	0.45		0.00002		0.57	0.01	16.44	0.2	0.21	0.0002	0.98	2922	38	2890	2	101
16.1	359	115	0.32		0.00002		0.53	0.01	14.92	0.2	0.20	0.0004	0.99	2755	37	2849	3	97
8.1	318	130	0.41		0.00006		0.51	0.01	14.18	0.2	0.20	0.0005	0.95	2666	36	2831	4	94
12.2	274	145	0.53		0.00025		0.52	0.01	14.23	0.2	0.20	0.0007	0.97	2708	37	2806	6	97
13.1	509	256	0.50		0.00003		0.52	0.01	13.94	0.2	0.20	0.0003	0.97	2683	35	2791	3	96
Weakly luminescent outer cores, faint planar banding																		
1.1	746	278	0.37		0.00005		0.56	0.01	15.84	0.3	0.20	0.0005	0.99	2874	50	2862	4	100
1.3	700	211	0.30		0.00006		0.53	0.01	14.83	0.3	0.20	0.0005	0.98	2755	48	2839	4	97
3.2	765	314	0.41		0.00003		0.55	0.01	15.49	0.3	0.20	0.0003	0.98	2841	49	2848	3	100
Weakly luminescent homogeneous core																		
15.1	456	91	0.20		0.00002		0.53	0.01	14.84	0.2	0.20	0.0004	0.98	2743	36	2849	3	96
Highly luminescent rims & grains																		
19.1	102	95	0.94		0.00025		0.51	0.01	12.24	0.2	0.17	0.0013	0.84	2659	39	2595	13	102
12.1	453	202	0.45		0.00005		0.44	0.01	9.99	0.1	0.16	0.0004	0.95	2366	31	2489	4	95
n-21.1	176	235	1.33	69	0.00003	0.04	0.45	0.01	10.15	0.1	0.16	0.0006	0.96	2411	25	2480	6	97
n-22.1	113	83	0.73	45	0.00003	0.04	0.46	0.01	10.52	0.1	0.16	0.0007	0.93	2452	23	2506	8	98
n-23.1	288	135	0.47	113	0.00001	0.01	0.46	0.01	10.41	0.1	0.17	0.0007	0.95	2429	25	2508	7	97
n-24.1	291	325	1.12	115	0.00001	0.02	0.46	0.01	10.38	0.1	0.16	0.0006	0.97	2447	25	2488	6	98
n-25.1	146	162	1.11	57	0.00003	0.05	0.46	0.01	10.17	0.1	0.16	0.0006	0.94	2428	23	2470	7	98
n-26.1	253	211	0.83	102	0.00001	0.01	0.47	0.01	10.55	0.1	0.16	0.0006	0.95	2483	22	2486	6	100
n-27.1	103	332	3.21	41	0.00005	0.07	0.46	0.01	10.24	0.1	0.16	0.0008	0.93	2442	24	2469	8	99
n-28.1	582	108	0.18	261	0.00001	0.01	0.52	0.01	13.65	0.2	0.19	0.0006	0.97	2704	24	2742	5	99
Overlaps																		
1.2	807	480	0.60		0.00008		0.56	0.01	15.89	0.3	0.21	0.0005	0.98	2863	50	2875	4	100
2.1	1217	139	0.11		0.00001		0.58	0.01	16.03	0.3	0.20	0.0002	0.97	2932	50	2840	2	103
17.1	328	150	0.46		0.00005		0.52	0.01	13.85	0.2	0.20	0.0005	0.98	2678	36	2785	4	96
4.2	451	188	0.42		0.00004		0.52	0.01	13.41	0.2	0.19	0.0004	1.00	2683	36	2728	4	98
20.1	1022	141	0.14		0.00001		0.51	0.01	12.56	0.2	0.18	0.0002	0.97	2651	35	2644	2	100

1 Uncertainties given at the one sigma level. 2. f206 % denotes the percentage of ^{206}Pb that is common Pb, *3* Correction for common Pb made using the measured $^{204}Pb/^{206}Pb$ ratio. *4* ρ = error correlation between $^{206}Pb/^{238}U$ and $^{207}Pb/^{235}U$ ratios. *5* Prefix "n-" indicates data collected in Session 2, *6* Gaps in graph are due to particular data not being available for the older analyses

Table 4 Summary of SHRIMP U/Pb zircon results for sample 78285005: Dallwitz Nunatak Orthogneiss

Grain. spot	U (ppm)	Th (ppm)	Th/U (ppm)	Pb*	$^{204}Pb/^{206}Pb$	f_{206} (%)	Radiogenic Ratios						ρ	Age (Ma)				Disc (%)
							$^{206}Pb/^{238}U$	±	$^{207}Pb/^{235}U$	±	$^{207}Pb/^{206}Pb$	±		$^{206}Pb/^{238}U$	±	$^{207}Pb/^{206}Pb$	±	
Oscillatory zoned cores																		
1.1	347	229	0.66		0.000079		0.61	0.02	18.57	0.65	0.22	0.0010	0.97	3060	104	2992	8	102
5.1	1100	163	0.15		0.000008		0.59	0.02	17.65	0.60	0.22	0.0005	0.99	2991	101	2956	4	101
9.1	208	207	1.00		0.000013		0.60	0.02	17.56	0.62	0.21	0.0012	0.96	3037	103	2918	9	104
18.1	622	288	0.46		0.000016		0.59	0.02	17.71	0.61	0.22	0.0008	0.98	2986	101	2965	6	101
24.1	759	341	0.45		0.000010		0.55	0.02	15.77	0.54	0.21	0.0008	0.99	2826	95	2888	6	98
25.1	602	182	0.30		0.000016		0.52	0.02	15.20	0.53	0.21	0.0010	0.97	2711	92	2911	7	93
26.1	684	241	0.35		0.000017		0.57	0.02	16.46	0.57	0.21	0.0010	0.98	2894	98	2910	8	99
n-40.1	440	204	0.46	225	0.000010	0.01	0.59	0.01	17.66	0.22	0.22	0.0014	0.85	3009	25	2946	10	102
Altered cores																		
2.1	147	93	0.63		0.000124		0.53	0.02	14.53	0.53	0.20	0.0017	0.93	2756	94	2805	14	98
3.1	7968	1027	0.13		0.000002		0.62	0.02	17.05	0.58	0.20	0.0002	0.99	3127	105	2809	2	111
8.1	821	263	0.03		0.000025		0.57	0.02	15.69	0.54	0.20	0.0006	0.98	2891	98	2834	5	102
10.1	509	328	0.64		0.000047		0.59	0.02	16.59	0.57	0.20	0.0007	0.98	3000	101	2850	6	105
11.1	2140	1225	0.57		0.000002		0.56	0.02	15.59	0.53	0.20	0.0004	0.99	2881	97	2831	3	102
23.1	650	223	0.34		0.000001		0.53	0.02	14.88	0.51	0.20	0.0008	0.99	2741	93	2855	6	96
28.1	2248	908	0.40		0.000001		0.56	0.02	15.59	0.53	0.20	0.0005	0.99	2869	97	2839	4	101
17.1 (r)	5846	115	0.04		0.000004		0.53	0.02	14.02	0.48	0.19	0.0003	0.98	2748	93	2753	3	100
19.1 (r)	649	79	0.12		0.000002		0.53	0.02	13.67	0.47	0.19	0.0007	0.98	2753	93	2707	7	102
21.1 (r)	960	286	0.30		0.000014		0.53	0.02	14.28	0.49	0.20	0.0006	0.98	2731	92	2795	5	98
27.1 (r)	1535	42	0.03		0.000006		0.51	0.02	13.18	0.45	0.19	0.0006	0.99	2643	89	2729	5	97
Weakly luminescent banded outer cores/rims																		
5.2	2594	90	0.04		0.000003		0.57	0.02	15.95	0.54	0.20	0.0003	0.99	2913	98	2846	3	102
7.2	2023	77	0.04		0.000007		0.55	0.02	15.31	0.52	0.20	0.0004	0.99	2831	95	2837	3	100
15.2	1624	61	0.04		0.000011		0.57	0.02	16.00	0.54	0.21	0.0004	0.99	2891	97	2866	4	101
17.2	2041	81	0.04		0.000027		0.57	0.02	16.27	0.55	0.21	0.0004	0.99	2904	97	2855	3	101
23.2	1634	56	0.03		0.000013		0.55	0.02	15.30	0.52	0.20	0.0005	0.99	2838	95	2831	4	100
11.2 (r)	2544	109	0.04		0.000004		0.47	0.02	11.35	0.39	0.17	0.0003	0.98	2490	84	2602	3	96
20.2 (r)	2715	91	0.03		0.000048		0.42	0.01	11.23	0.38	0.19	0.0004	0.99	2257	76	2778	4	81
n-41.1 (r)	490	353	0.72	242	0.000011	0.01	0.57	0.01	16.66	0.27	0.21	0.0019	0.84	2924	32	2909	15	101
Weakly luminescent, homogeneous rims																		
3.2	2494	104	0.04		0.000007		0.51	0.02	12.73	0.43	0.18	0.0003	1.00	2674	90	2649	3	101
10.2	1809	96	0.05		0.000001		0.52	0.02	13.59	0.46	0.19	0.0004	0.99	2714	91	2726	3	100
21.2	2208	82	0.04		0.000073		0.50	0.02	12.80	0.44	0.18	0.0004	0.98	2631	89	2690	4	98
Weakly-moderately luminescent, planar banded/sector zoned grains																		
12.1	1361	262	0.19		0.000017		0.45	0.02	9.94	0.34	0.16	0.0005	0.99	2382	80	2468	5	97
16.1	2356	334	0.14		0.000008		0.47	0.02	10.79	0.37	0.17	0.0003	0.98	2497	84	2511	4	99
19.2	1279	279	0.22		0.000003		0.47	0.02	10.60	0.36	0.16	0.0005	0.99	2490	84	2487	6	100
22.1	6410	539	0.08		–		0.50	0.02	11.15	0.38	0.16	0.0002	0.99	2600	87	2484	2	105
25.2	2453	153	0.06		0.000004		0.47	0.02	10.49	0.36	0.16	0.0004	0.98	2474	83	2482	5	100
29.1	1046	359	0.34		0.000008		0.45	0.02	10.12	0.35	0.16	0.0007	0.97	2415	81	2470	7	98
30.1	882	265	0.30		0.000013		0.45	0.02	10.16	0.35	0.16	0.0008	0.98	2399	81	2490	9	96
n-31.1	1314	173	0.13	525	0.000005	0.01	0.46	0.01	10.79	0.13	0.17	0.0008	0.92	2461	22	2542	8	97
n-32.1	1847	176	0.10	732	0.000002	< 0.01	0.46	0.00	10.54	0.11	0.17	0.0003	0.99	2446	21	2514	3	97
n-33.1	1264	318	0.25	519	0.000009	0.01	0.48	0.01	10.75	0.13	0.16	0.0006	0.95	2520	23	2487	6	101
n-34.1	1839	227	0.12	744	0.000002	< 0.01	0.47	0.01	10.41	0.15	0.16	0.0006	0.97	2486	29	2461	6	101
n-35.1	1622	194	0.12	658	0.000002	< 0.01	0.47	0.00	10.66	0.11	0.16	0.0004	0.97	2493	21	2495	4	100

Table 4 (Contd.)

Grain. spot	U (ppm)	Th (ppm)	Th/U (ppm)	Pb*	$^{204}Pb/^{206}Pb$	f_{206} (%)	Radiogenic Ratios						ρ	Age (Ma)				Disc (%)
							$^{206}Pb/^{238}U$	±	$^{207}Pb/^{235}U$	±	$^{207}Pb/^{206}Pb$	±		$^{206}Pb/^{238}U$	±	$^{207}Pb/^{206}Pb$	±	
n-36.1	1033	142	0.14	418	0.000004	0.01	0.47	0.01	10.49	0.13	0.16	0.0009	0.91	2485	23	2474	9	100
n-37.1	1302	226	0.17	529	0.000002	< 0.01	0.47	0.00	10.49	0.11	0.16	0.0003	0.99	2497	21	2464	3	101
n-38.1	914	166	0.18	383	0.000029	0.04	0.49	0.01	10.79	0.12	0.16	0.0003	0.98	2563	23	2459	4	104
n-39.1	1901	425	0.22	749	0.000003	< 0.01	0.46	0.00	10.19	0.10	0.16	0.0002	0.99	2433	21	2469	2	99
Overlaps																		
4.1	2255	288	0.13		0.000093		0.63	0.02	20.25	0.69	0.23	0.0004	0.99	3143	106	3077	3	102
6.1	969	89	0.09		0.000027		0.69	0.02	30.76	1.05	0.32	0.0007	0.98	3394	114	3579	3	95
7.1	965	87	0.09		0.000019		0.61	0.02	19.84	0.68	0.23	0.0006	0.98	3083	104	3084	4	100
13.1	702	58	0.08		0.000016		0.57	0.02	15.25	0.52	0.19	0.0006	0.99	2919	98	2768	5	105
14.1	82	360	0.44		0.000011		0.65	0.02	20.04	0.68	0.22	0.0006	0.99	3218	108	3013	4	107
14.2	2917	127	0.04		0.000003		0.52	0.02	12.74	0.43	0.18	0.0003	1.00	2698	91	2632	3	103
15.1	975	30	0.03		0.000014		0.54	0.02	14.12	0.48	0.19	0.0005	0.99	2775	93	2744	5	101
20.1	3357	267	0.08		0.000006		0.57	0.02	16.84	0.57	0.21	0.0003	0.99	2911	98	2935	3	99

1. Uncertainties given at the one sigma level. 2. f206 % denotes the percentage of ^{206}Pb that is common Pb
3. Correction for common Pb made using the measured $^{204}Pb/^{206}Pb$ ratio. 4. ρ = error correlation between $^{206}Pb/^{238}U$ and $^{207}Pb/^{235}U$ ratios. 5. Prefix "n-" indicates data collected in Session 2; (r) indicates data rejected from pooled age calculations. 6. Gaps in graph are due to particular data not being available for the older analyses

Eight analyses (disturbed grains: 8.1, 16.1; weakly luminescent outer cores and rims: 1.1, 1.2, 1.3, 2.1, 3.2, 15.1), form a dominant cluster that is mildly discordant. This cluster defines a chord with an upper intercept age of 2,854 ± 14 Ma (lower intercept = 476 ± 690 Ma, MSWD = 3.1; Fig. 7c), similar to the age inferred by Harley and Black (1997; 2,847 ± 11 Ma) to reflect an episode of isotopic resetting.

Session 2 analyses focussed on planar/sector zoned, moderate-highly luminescent zircon grains and highly luminescent rims. These grains and rims have Th/U ratios that are scattered between 0.45 and 1.5, except for a single analysis with Th/U = 3.2 (n27.1). It is notable that all of the measured Th/U are significantly higher than the range of Th/U inferred by some authors to be characteristic of metamorphic zircon (e.g., Rubatto 2002). All but one analysis (n28.1; $^{207}Pb/^{206}Pb$ age = 2,742 ± 5 Ma) cluster close to ca. 2,490 Ma and define a slightly discordant array that has an upper intercept with the concordia curve at 2,488 ± 28 Ma (MSWD = 2.2, $n = 8$; Fig. 7d). A lower intercept age of 99 ± 2,000 Ma suggests discordance due to recent Pb-loss. The data produce an average $^{207}Pb/^{206}Pb$ age of 2,487 ± 10 Ma (95% confidence interval, MSWD = 4.1; Fig. 7d).

Dallwitz Nunatak granitic orthogneiss: sample 78285005

The data from the Dallwitz Nunatak sample comprise 53 analyses (11 new analyses) that scatter along concordia between ca. 3,000 to 2,450 Ma, with one outlier at ca. 3,579 Ma (Fig. 8a, b). Harley and Black (1997) interpreted that cores with ages older than ca. 2,850 Ma were xenocrystic in origin, and pooled analyses of "distinct cores" and "strongly zoned rims" to calculate a single age of 2,850 +40/−20 Ma for the crystallisation of the orthogneiss precursor. However, using SEM images obtained in the present study, data from distinct zoning types that are interpreted to be unrelated have been separated. Oscillatory zoned grains have Th/U ratios that vary between 0.14 and 0.9, typical of igneous zircon (Fig. 8b, Table 4). A population of eight analyses (including one new analysis, n40.1) have $^{207}Pb/^{206}Pb$ ages of between 2,992 and 2,910 Ma, correlating with a minor scatter along the concordia curve. The data array has an upper intercept with the concordia curve at 2,933 ± 25 Ma (MSWD = 1.3; Fig. 8c, inset). However, the scatter along concordia indicates minor isotopic resetting, suggesting the ca. 2,933 Ma age may reflect a minimum age for these oscillatory zoned cores.

Twenty-five analyses that comprise altered cores and weakly luminescent overgrowths (planar banded and homogeneous; Fig. 4a, b, d) form a scatter along the concordia curve between 2,900 and 2,650 Ma. Eleven altered cores have Th/U values between 0.03 and 0.64 that are similar to or lower than the range observed for igneous zircon cores in this sample. Weakly luminescent overgrowths have steep MREE-depleted, HREE-en-

Table 5 Summary of SHRIMP U/Pb zircon results for sample 80285037: Zircon Point Paragneiss

Grain. Spot	U (ppm)	Th (ppm)	Th/U	Pb* (ppm)	$^{204}Pb/^{206}Pb$	f_{206} (%)	Radiogenic Ratios						ρ	Age (Ma)				Disc (%)
							$^{206}Pb/^{238}U$	±	$^{207}Pb/^{235}U$	±	$^{207}Pb/^{206}Pb$	±		$^{206}Pb/^{238}U$	±	207Pb/206Pb	±	
Oscillatory zoned - minor alteration																		
1.1	316	114	0.36		0.000083		0.49	0.01	13.15	0.41	0.20	0.0007	0.11	2553	77	2795	6	91
4.1	2007	988	0.49		0.000009		0.55	0.02	14.95	0.45	0.20	0.0003	1.00	2830	85	2799	2	101
4.2	483	221	0.46		0.000005		0.54	0.02	14.42	0.44	0.20	0.0006	0.10	2764	84	2787	5	99
5.1	1394	692	0.50		0.000019		0.54	0.02	14.20	0.43	0.19	0.0003	0.05	2770	83	2758	3	100
6.1	376	149	0.40		0.000037		0.55	0.02	16.64	0.51	0.22	0.0005	0.07	2831	85	2972	4	95
7.1	858	337	0.39		0.000016		0.53	0.02	14.66	0.44	0.20	0.0003	1.00	2724	82	2843	3	96
8.1	908	500	0.55		0.000002		0.50	0.01	12.55	0.38	0.18	0.0003	0.05	2594	78	2686	3	97
9.1	895	410	0.46		0.000020		0.56	0.02	15.98	0.48	0.21	0.0003	1.00	2857	86	2888	3	99
9.2	1265	547	0.43		0.000004		0.56	0.02	15.70	0.48	0.20	0.0003	0.05	2870	86	2850	3	101
15.1	385	133	0.35		0.000030		0.56	0.02	15.58	0.48	0.20	0.0006	0.10	2854	86	2849	5	100
16.1	497	215	0.43		0.000021		0.48	0.01	11.74	0.36	0.18	0.0005	0.09	2535	76	2623	4	97
20.1	1169	612	0.52		0.000025		0.55	0.02	15.21	0.46	0.20	0.0003	0.05	2826	85	2829	3	100
21.1	1725	729	0.42		0.000004		0.58	0.02	16.29	0.49	0.20	0.0003	0.05	2957	89	2850	3	104
22.1	1639	781	0.48		–		0.57	0.02	15.70	0.48	0.20	0.0003	0.05	2890	87	2836	3	102
23.1	474	187	0.40		0.000003		0.56	0.02	15.93	0.49	0.20	0.0006	0.10	2883	87	2864	5	101
24.1	1110	591	0.53		0.000003		0.54	0.02	14.91	0.45	0.20	0.0003	0.05	2790	84	2823	3	99
25.1	667	285	0.43		0.000021		0.54	0.02	14.51	0.44	0.20	0.0005	0.08	2766	84	2795	4	99
28.1	796	347	0.44		0.000013		0.50	0.02	11.46	0.35	0.17	0.0006	0.12	2626	79	2510	6	105
30.1	1407	625	0.44		0.000008		0.55	0.02	14.02	0.42	0.19	0.0003	1.00	2820	85	2700	3	104
Intensely altered cores																		
12.1	608	228	0.38		0.000020		0.49	0.01	11.56	0.35	0.17	0.0004	0.08	2559	77	2577	4	99
18.1	474	204	0.43		0.000085		0.35	0.01	6.23	0.19	0.13	0.0005	0.13	1944	59	2076	8	94
19.1	448	195	0.44		0.000003		0.57	0.02	16.23	0.50	0.21	0.0006	0.09	2890	87	2891	4	100
26.1	301	139	0.46		0.000036		0.55	0.02	14.75	0.46	0.19	0.0010	0.17	2831	86	2776	8	102
27.1	429	195	0.45		0.000004		0.56	0.02	15.55	0.48	0.20	0.0006	0.10	2857	86	2844	5	100
31.1	572	127	0.22		0.000031		0.49	0.01	11.88	0.36	0.18	0.0005	0.09	2560	77	2621	4	98
Group 1 - Weakly to moderately luminescent grains; planar banded and sector zoned																		
2.1	498	184	0.37		0.000068		0.40	0.01	8.52	0.26	0.15	0.0005	0.11	2184	66	2381	6	92
3.1	1206	173	0.14		0.000017		0.40	0.01	8.61	0.26	0.16	0.0004	0.09	2179	66	2404	4	91
10.1	573	206	0.36		0.000025		0.49	0.01	11.42	0.35	0.17	0.0004	0.08	2556	77	2559	4	100
10.2	551	195	0.35		0.000018		0.49	0.01	11.75	0.36	0.17	0.0004	0.08	2588	78	2580	4	100
13.1	927	250	0.27		0.000004		0.46	0.01	10.66	0.32	0.17	0.0003	1.00	2446	74	2535	3	97
n-33.1	1022	509	0.50	415	0.000004	0.01	0.47	0.00	10.77	0.12	0.17	0.0007	0.93	2497	21	2509	7	100
n-37.1	580	165	0.28	250	0.000004	0.01	0.50	0.01	11.58	0.13	0.17	0.0004	0.98	2618	23	2533	4	103
n-32.1 (r)	974	279	0.29	323	0.000008	0.01	0.39	0.00	7.17	0.09	0.13	0.0005	0.95	2107	22	2158	7	98
n-48.1 (r)	1082	506	0.47	437	–	<0.01	0.47	0.00	10.21	0.11	0.16	0.0003	0.98	2484	22	2430	3	102
Group 2 - Moderately luminescent rims; planar banded																		
5.2	221	391	1.76		0.000058		0.47	0.01	10.50	0.33	0.16	0.0008	0.16	2471	75	2486	9	99
6.2	331	144	0.44		0.000034		0.46	0.01	10.51	0.32	0.17	0.0004	0.08	2431	73	2521	4	96
27.2	607	238	0.39		0.000010		0.45	0.01	10.46	0.33	0.17	0.0008	0.15	2416	73	2525	8	96
n-33.2	179	247	1.38	71	0.000090	0.13	0.46	0.01	10.26	0.14	0.16	0.0012	0.84	2441	24	2473	13	99
n-34.1	358	194	0.54	150	0.000008	0.01	0.49	0.01	10.94	0.13	0.16	0.0008	0.91	2560	23	2484	9	103
n-39.1	729	190	0.26	301	0.000000	<0.01	0.48	0.00	10.83	0.12	0.16	0.0005	0.95	2528	21	2493	5	101
n-43.1	604	157	0.26	263	0.000007	0.01	0.51	0.01	11.59	0.15	0.17	0.0008	0.92	2640	26	2519	8	105
n-44.1	540	173	0.32	232	0.000007	0.01	0.50	0.01	11.66	0.14	0.17	0.0009	0.91	2618	23	2546	8	103

Table 5 Continued

Grain. Spot	U (ppm)	Th (ppm)	Th/U	Pb* (ppm)	$^{204}Pb/^{206}Pb$	f_{206} (%)	Radiogenic Ratios						ρ	Age (Ma)				Disc (%)
							$^{206}Pb/^{238}U$	±	$^{207}Pb/^{235}U$	±	$^{207}Pb/^{206}Pb$	±		$^{206}Pb/^{238}U$	±	207Pb/206Pb	±	
n-35.1 (r)	547	185	0.34	185	0.000002	<0.01	0.39	0.01	7.71	0.24	0.14	0.0024	0.83	2145	46	2247	29	95
Group 3 - Highly luminescent outer cores and rims; planar banded and sector zoned																		
n-38.1	186	279	1.50	80	0.000009	0.01	0.50	0.01	11.40	0.16	0.17	0.0015	0.76	2607	23	2517	16	104
n-40.1	228	265	1.16	95	0.000015	0.02	0.48	0.01	10.83	0.14	0.16	0.0005	0.97	2545	26	2480	5	103
n-41.1	232	306	1.32	95	0.000027	0.04	0.48	0.01	10.67	0.13	0.16	0.0008	0.90	2520	22	2475	9	102
n-42.1	234	261	1.11	102	0.000012	0.02	0.51	0.01	11.55	0.16	0.16	0.0010	0.89	2652	26	2504	10	106
n-46.1	264	459	1.74	114	0.000020	0.03	0.50	0.01	11.48	0.14	0.17	0.0008	0.91	2622	24	2516	9	104
n-49.1	225	361	1.60	98	0.000002	<0.01	0.51	0.01	11.40	0.14	0.16	0.0010	0.88	2636	24	2494	10	106
n-36.1 (r)	249	400	1.60	95	0.000005	0.01	0.44	0.01	9.05	0.12	0.15	0.0006	0.95	2356	24	2331	7	101
n-45.1 (r)	233	311	1.33	93	0.000009	0.01	0.46	0.01	9.96	0.13	0.16	0.0006	0.95	2452	26	2414	7	102
Group 4- Weakly luminescent rims, homogeneous																		
7.2	725	159	0.22				0.46	0.01	10.52	0.32	0.17	0.0004	0.08	2429	73	2524	4	96
n-42.2	1354	77	0.06	577	0.000003	<0.01	0.50	0.01	11.53	0.14	0.17	0.0011	0.85	2596	22	2545	10	102
Overlaps																		
11.1	378	35	0.09		0.000045		0.54	0.02	14.97	0.46	0.20	0.0005	0.08	2801	84	2822	4	99
14.1	512	119	0.23		0.000034		0.37	0.01	7.17	0.22	0.14	0.0005	0.12	2045	62	2218	6	92
17.1	493	185	0.38		0.000004		0.36	0.01	6.95	0.21	0.14	0.0004	0.09	1962	59	2249	5	87
26.2	856	346	0.41		0.000016		0.51	0.02	11.41	0.35	0.16	0.0006	0.12	2635	79	2495	6	106
29.1	809	207	0.26		0.000007		0.46	0.01	9.86	0.30	0.16	0.0005	0.11	2438	74	2408	5	101

1 Uncertainties given at the one sigma level. *2* f206 % denotes the percentage of ^{206}Pb that is common Pb. *3* Correction for common Pb made using the measured $^{204}Pb/^{206}Pb$ ratio. *4* ρ = error correlation between $^{206}Pb/^{238}U$ and $^{207}Pb/^{235}U$ ratios. *5* Prefix "n-" indicates data collected in Session 2; (*r*) indicates data rejected from pooled age calculations as referred to in the text. *6* Gaps in graph are due to particular data not being available for the older analyses

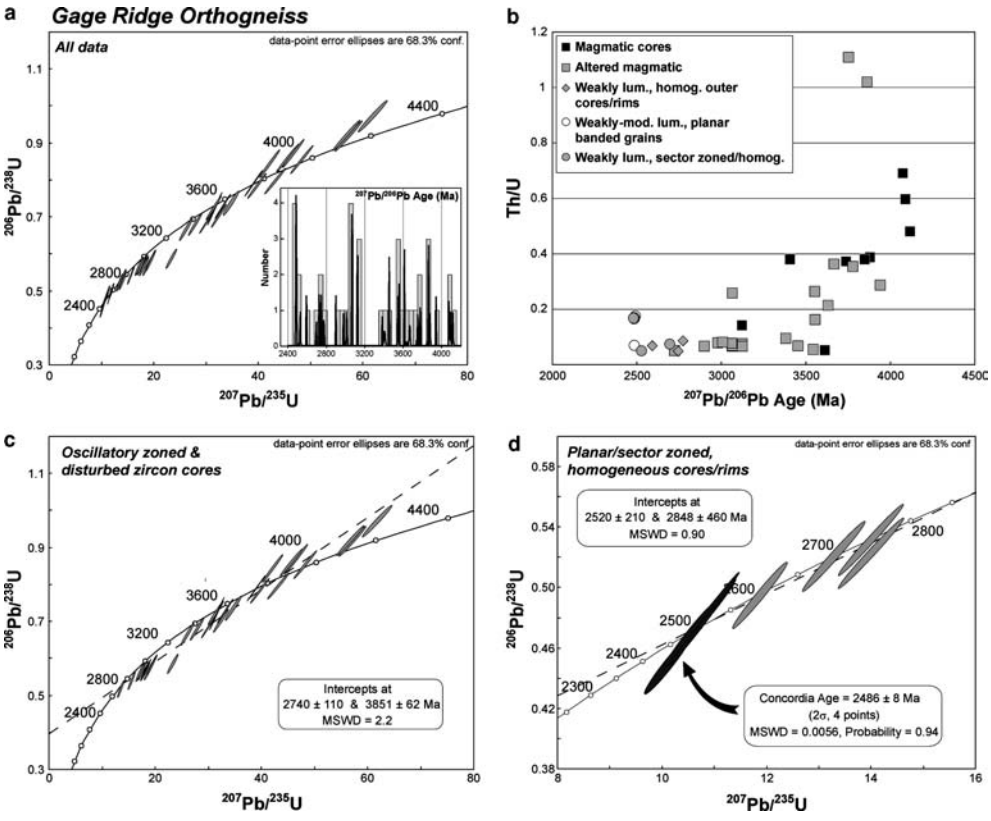

Fig. 6 U–Pb isotope data from Gage Ridge orthogneiss zircon grains. **a** Conventional concordia diagram showing all data. *Inset*: Cumulative probability diagram of $^{207}Pb/^{206}Pb$ ages. **b** Th/U versus $^{207}Pb/^{206}Pb$ age for zircons analysed by SHRIMP. **c** Conventional concordia diagram showing data from oscillatory zoned and altered cores: data define a Pb-loss array which has an upper intercept with concordia at 3,851 ± 62 Ma, a minimum age for the crystallisation of the orthogneiss protolith. **d** Conventional concordia diagram for data from planar banded and sector zoned zircons, plus homogeneous cores and rims. Four analyses form a cluster at the bottom of a Pb-loss array, and reflect new growth of zircon at 2,486 ± 8 Ma

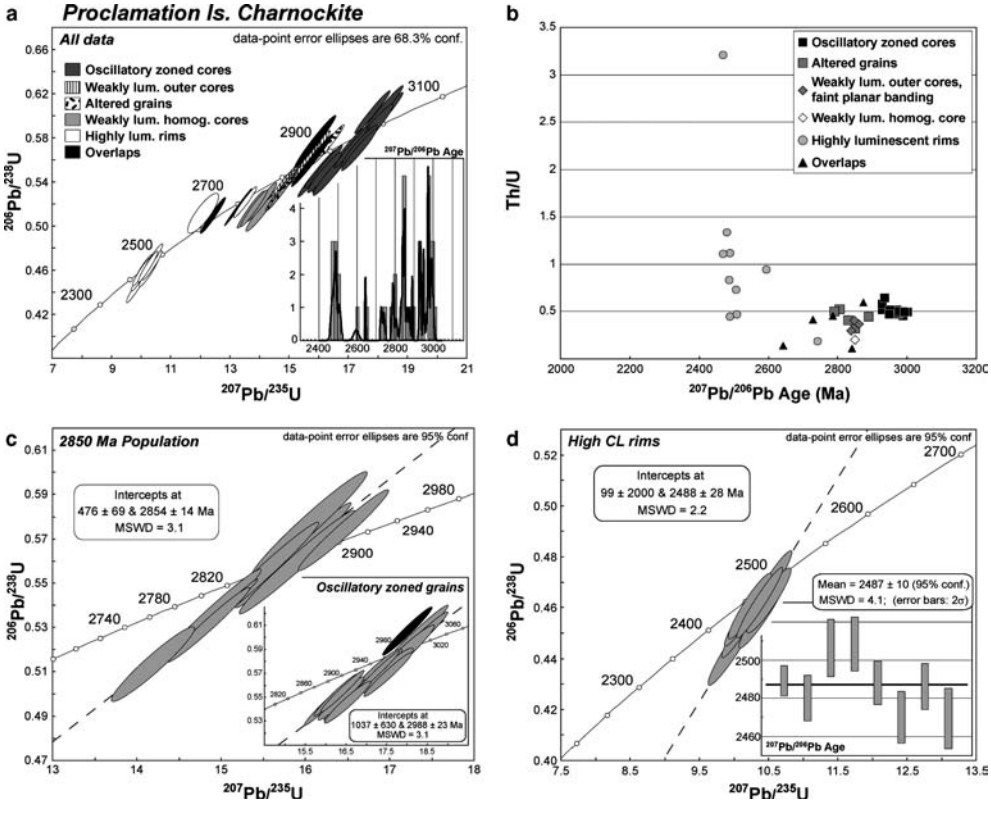

Fig. 7 U–Pb isotope data from Proclamation Island charnockite zircon grains. **a** Conventional concordia diagram showing all data. *Inset*: Cumulative probability diagram of $^{207}Pb/^{206}Pb$ ages. **b** Th/U vs $^{207}Pb/^{206}Pb$ age for zircons analysed by SHRIMP. **c** Conventional concordia diagram showing data from weakly luminescent, banded overgrowths and altered grains that form a near to concordant cluster that intercepts the concordia curve at 2,854 ± 14 Ma. *Inset:* data from 2,988 ± 23 Ma oscillatory zoned cores. Note: the black in-filled ellipse reflects data rejected from the error-weighted regression. **d** Conventional concordia diagram for data from highly luminescent grains and rims. Data define a slightly discordant cluster that intersects the concordia curve at 2,488 ± 28 Ma. *Inset:* Weighted average of $^{207}Pb/^{206}Pb$ ages for the same data population: 2,487 ± 10 Ma

riched patterns (Yb/Gd≈67) and a narrow range of Th/U ratios (0.03–0.05). A single analysis (41.1), which has higher Th/U (0.7) and old $^{207}Pb/^{206}Pb$ age (ca. 2,909 Ma), may be a partially recrystallised igneous zircon rim, rather than a metamorphic overgrowth. A group of 12 analyses define a near to concordant cluster

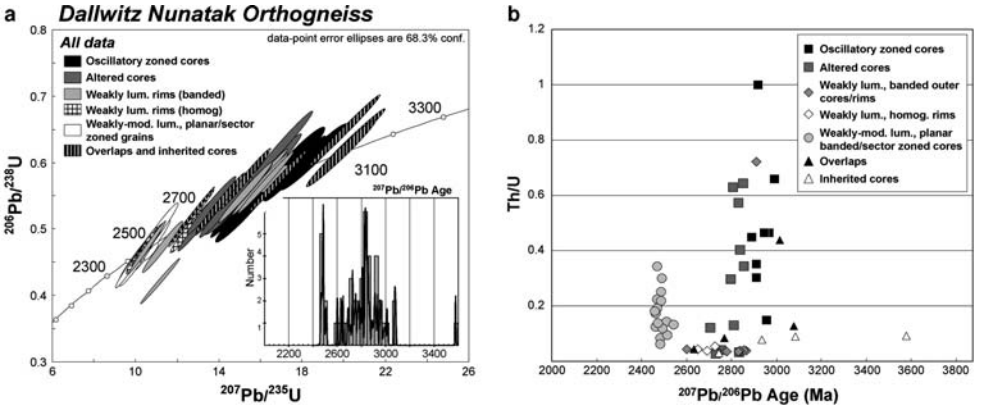

Fig. 8 U–Pb isotope data from Dallwitz Nunatak orthogneiss zircon grains. **a** Conventional concordia diagram showing all data. *Inset*: Cumulative probability diagram of $^{207}Pb/^{206}Pb$ ages. **b** Th/U vs $^{207}Pb/^{206}Pb$ age for zircons analysed by SHRIMP. **c** Conventional concordia diagram showing data banded cores and overgrowths and altered grains. Data define a near to concordant cluster that intercepts the concordia curve at 2,842 ± 16 Ma. *Inset*: data from 2,933 ± 25 Ma oscillatory zoned cores reflects a minimum age for the crystallisation of the orthogneiss protolith. **d** Conventional concordia diagram for data from weakly-moderately luminescent, planar banded and sector zoned cores and rims. Data define a cluster that intersects the concordia curve at 2,485 ± 14 Ma. *Inset*: Weighted average of $^{207}Pb/^{206}Pb$ ages for the same data population: 2,480 ± 9.6 Ma

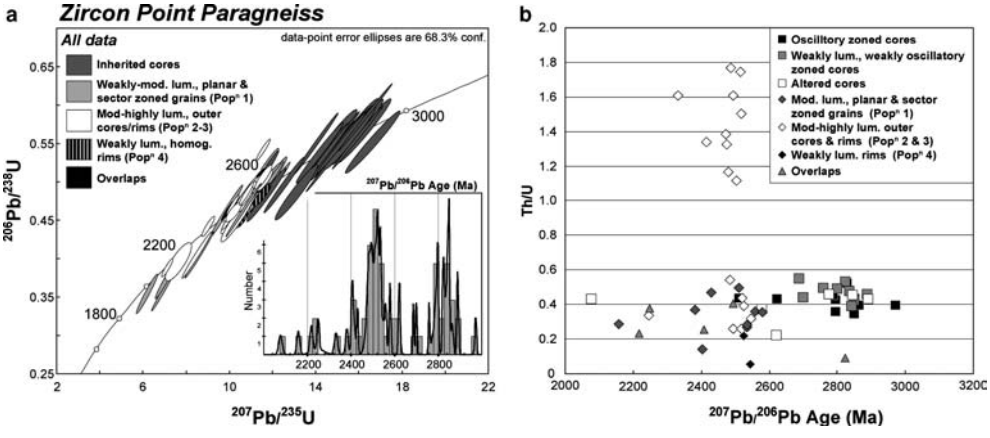

Fig. 9 U–Pb isotope data from Zircon Point paragneiss zircon grains. **a** Conventional concordia diagram showing all data. *Inset*: Cumulative probability diagram of $^{207}Pb/^{206}Pb$ ages. **b** Th/U vs $^{207}Pb/^{206}Pb$ age for zircons analysed by SHRIMP

at ca. 2,840 Ma; data that form excess scatter around this group (ten analyses) were rejected from age estimates. The clustered data array has an upper intercept with concordia at 2,842 ± 16 Ma (lower intercept = −159 ± 1,100 Ma; MSWD = 1.8; Fig. 8c).

Sixteen analyses from weakly to moderately luminescent, planar banded and sector zoned grains (Fig. 4e), including nine new analyses, have scattered Th/U ratios between 0.06–0.34 (Fig. 8b), generally higher than the range typically inferred for metamorphic zircon. These grains have distinct, HREE-depleted compositions compared with older zircon grains (Fig. 4e). Their $^{207}Pb/^{206}Pb$ ages fall between 2,459 and 2,542 Ma, with only minor normal discordance (< 5%). The data array has an upper intercept with the concordia curve at 2,485 ± 14 Ma (MSWD = 2.1; Fig. 8d) and a lower intercept at 281 ± 1,100 Ma, consistent with recent Pb-loss. The data produce an average $^{207}Pb/^{206}Pb$ age of 2,480 ± 10 Ma (95% confidence interval, MSWD = 24; Fig. 8d).

Zircon Point paragneiss: sample 80285037

Data from this sample comprise 56 analyses, of which 23 are from inherited cores (17 oscillatory zoned, six altered) and five are from overlapping areas between zones. Inherited grains have $^{207}Pb/^{206}Pb$ ages that are scattered between 2,970 and 2,070 Ma, with all but three analyses greater than 2,600 Ma (Table 5). The scatter in

ages (Fig. 9a) precludes any attempt to accurately define the age of source rocks and is inferred to reflect igneous zircon ages that were partially reset by metamorphism between 2,550 and 2,450 Ma. The second zircon group comprises 28 analyses, including 20 new analyses from Populations 1–4, as previously defined from textural criteria. Clusters of individual ages overlap between populations. However, the four different zircon types described above have distinct and systematic textural contexts and contrasting REE patterns. Hence data from each population should be considered separately.

Population 1 zircon grains ($n = 9$), which have the highest REE concentrations of the four populations, have Th/U ratios of between 0.14 and 0.50 (Fig. 9b). From this population, two analyses were rejected for excess scatter (32.1, 48.1: filled black ellipses in Fig. 10a), with the remaining data defining an array that intersects the concordia curve at 2,543 ± 41 Ma (MSWD = 2.8; $n = 7$). The degree of discordance within this data population precludes the calculation of an average $^{207}Pb/^{206}Pb$ age. From Population 2 ($n = 9$), a single data point was rejected for excess deviation (35.1: filled black ellipse in Fig. 10b). The remaining data have Th/U ratios that are generally between 0.26 and 0.54, with a single analysis at 1.8, and are near to concordant or concordant. These data have an upper intercept with the concordia curve at 2,505 ± 26 Ma (MSWD = 3.7; $n = 8$). The weighted average of $^{207}Pb/^{206}Pb$ ages is 2,511 ± 17 Ma (95% confidence interval, MSWD = 9.1; Fig. 10b, inset). Population 3 analyses ($n = 8$) have high Th/U ratios of between 1.1 and 1.7, well outside the range that many workers consider typical for metamorphic zircon. From this Population 2 analyses were omitted from the age estimate due to excess scatter (36.1, 45.1: filled black ellipses in Fig. 10c). The remaining data form an array that intercepts the concordia curve at 2,450 ± 46 Ma (MSWD = 0.99; $n = 6$). The weighted average of $^{207}Pb/^{206}Pb$ ages is 2,490 ± 17 Ma (95% confidence interval, MSWD = 4.2; Fig. 10c). Two analyses were also taken from relatively homogeneous, weakly luminescent zircon rims around highly luminescent outer cores and rims (Population 4). The $^{207}Pb/^{206}Pb$ ages obtained on these two spots are older than the group age for Population 3 zircon (7.2: 2,524 ± 4 Ma, Th/U = 0.22; n42.2: 2,545 ± 10 Ma, Th/U = 0.06; Table 5).

All data in Population 3 and half the data from Population 2 are reversely discordant, the reasons for which are not clear. As the highly luminescent zircon from Population 3 is low in U (< 262 ppm) and should not have undergone intense metamictisation, reverse discordance is not likely to have resulted from matrix sputtering effects during analysis (as proposed by McLaren et al. 1994; Black et al. 1986a). In addition, the Th and U composition of grains in Population 2 are not significantly different to the FC1 standard that is used as a Pb/U reference. Moreover, analyses of the FC1 standard during the session that targeted Zircon Point grains are all concordant or normally discordant. This suggests that reverse discordance is not an obvious instrument

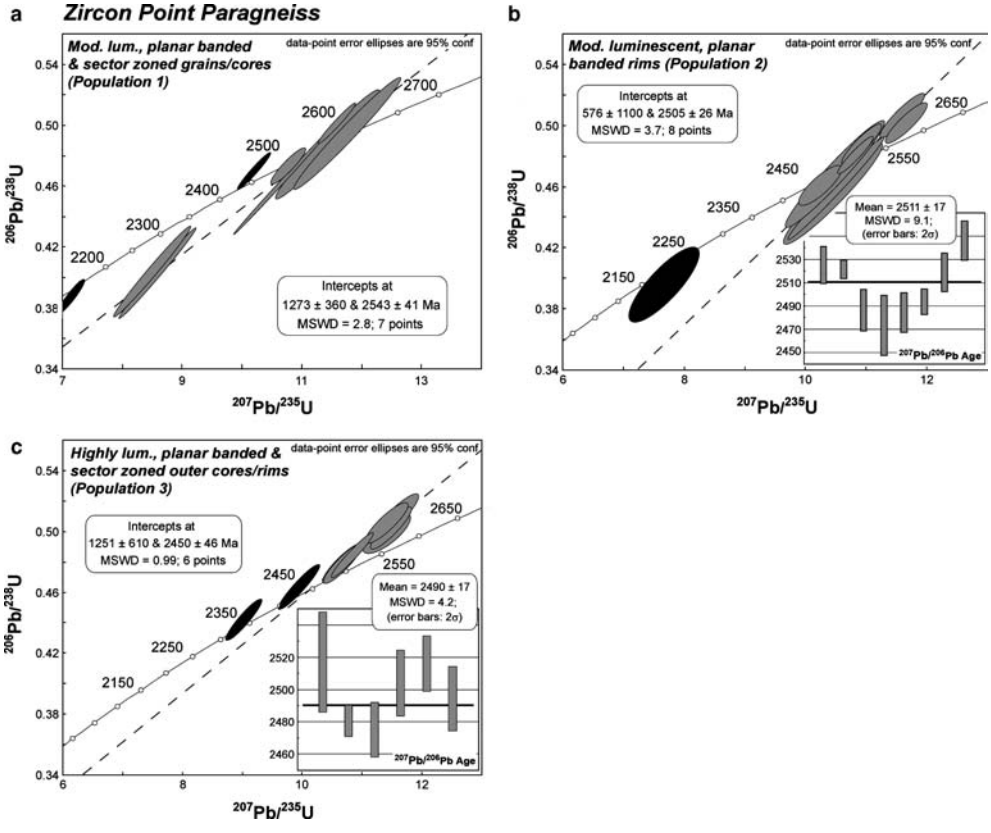

Fig. 10 **a** Conventional concordia diagram showing data from "Population 1" zircon grains (weakly luminescent, planar banded and sector zoned grains/cores). Note that the black in-filled ellipses reflect data rejected from the error-weighted regression. **b** Conventional concordia diagram showing data from "Population 2" zircon grains (moderately luminescent, planar banded rims). *Inset:* Weighted average of $^{207}Pb/^{206}Pb$ ages for the same data population: 2,511 ± 17 Ma. **c** Conventional concordia diagram showing data from "Population 3" zircon grains (highly luminescent, planar banded rims and sector zoned outer cores and rims). *Inset*: Weighted average of $^{207}Pb/^{206}Pb$ ages for the same data population: 2,490 ± 17 Ma

problem or a result of poor calibration, but reflects a process inherent to the zircon analysed. Based on this problem, the weighted average $^{207}Pb/^{206}Pb$ age for Population 3 is preferred.

Discussion

Integration of zircon internal zoning, REE and U/Pb isotopic data presented above allows for clarification and re-interpretation of the early magmatic and metamorphic history of the Napier Complex (Table 6). This re-interpretation is necessarily independent of any inferences that may be made on the basis of zircon Th/U characteristics, as from the data presented above it is clear that the interpretation of zircon as "metamorphic" or "magmatic" based on its preserved Th/U is highly suspect. For example, the Population 3 zircons from the *Zircon Point paragneiss*, interpreted as metamorphic based on their textural and REE features, preserve high Th/U (1.1–1.7) that are well outside the range often quoted for "metamorphic" zircon (0.01–0.06; e.g., Rubatto 2002). As the Th/U of zircon grown or modified during metamorphism is likely to be controlled by local chemical environment, competing accessory mineral formation, the presence of fluid or melt, and reaction relations it is not valid to assume a simple relation between Th/U and zircon origin.

The ca. 2,990 Ma magmatic episode in the Napier Complex

The ca. 2,990 Ma age for oscillatory zoned zircon cores from the Proclamation Charnockite confirms the original interpretation by Harley and Black (1997) for crystallisation of this rock at that time. However, the interpretation of the intrusion age for the Dallwitz Nunatak orthogneiss must be re-considered. Magmatic zircon cores have $^{207}Pb/^{206}Pb$ ages ranging between 2,990 and 2,890 Ma reflecting a degree of isotopic mobility, and it is possible that these grains are inherited xenocrysts that, therefore, do not reflect the age of the protolith to the orthogneiss (e.g., Harley and Black 1997). However, conformable zoning patterns between cores and rims in many grains (e.g., Fig. 4a) suggest that these cores grew during the crystallisation of the protolith. A chord through the data from these grains has an imprecise lower intercept age of ca. 1,500 Ma, which based on current geochronological data from the Napier Complex is geologically meaningless. Hence, it is probable that the isotopic disturbance reflects more than one Pb-loss event. This, combined with minor scatter along the concordia curve, suggests that the ca. 2,930 Ma upper intercept age for these data can only be regarded as a *minimum* estimate of the crystallisation of these grains. A better estimate for the age of zircon crystallisation may be equivalent to the age derived from the Proclamation Charnockite, ca. 2,990 Ma, which is also the age of the oldest oscillatory zoned grain in the Dallwitz Nunatak population (1.1). We now link the age of emplacement of the precursor to the Dallwitz Nunatak orthogneiss to this ca. 2,990 Ma magmatic episode. This age is older than the ca. 2,850 Ma age proposed by Harley and Black (1997) for emplacement of the precursor to the Dallwitz Nunatak orthogneiss. Hence, there is no evidence from the three orthogneisses studied here for an igneous event at ca. 2,850 Ma. However, this event is supported by the observation of ca. 2,855 Ma inherited zircon grains in the Zircon Point paragneiss and ca. 2,830 Ma igneous zircons from granitic gneiss (Suzuki 2000) and tonalite (Hokada et al. 2003) from Mt Riiser Larsen.

The data presented here also provides cause to review the early metamorphic history and reconsider the suggestion of a metamorphic event affecting the Napier Complex at ca. 3,000–2,980 Ma. Early Rb/Sr and Sm/Nd data suggested the occurrence of a crustal forming event and/or metamorphic modification of protoliths between 3,100 and 2,900 Ma (Sheraton and Black 1983; Black et al. 1986a, 1986b). A possible thermal event at this time may also be evidenced by zircon overgrowths in orthogneiss (ca. 2,948 Ma; Black et al. 1986a; Black 1988) and by disturbance of early Archaean zircons (ca. 3,850 Ma) at Mt Sones. Moreover, the Proclamation Island charnockite was originally interpreted to be syn-deformational (Black et al. 1986b) thereby apparently defining the timing of a "D_1/M_1" event (Harley and Black 1997). However, there is no evidence for metamorphic zircon of this age in the Proclamation Island charnockite. As orthopyroxene was probably present and garnet absent during all stages of the metamorphic evolution of the Proclamation Island charnockite, it is difficult to chemically link zircon growth to any particular phase of fabric development. Given that the field interpretation of syn-deformation intrusives is commonly inconclusive, as demonstrated below for the Dallwitz Nunatak orthogneiss, there is no substantial proof that a tectonothermal event accompanied magmatism at ca. 2,990 Ma.

The ca. 2,850–2,840 Ma high-*T*/low-*P* event

Weakly luminescent, planar banded or homogeneous outer cores and rims 2,850–2,840 Ma in age are interpreted to reflect metamorphic growth of zircon and are found in both Proclamation Island charnockite and Dallwitz Nunatak orthogneiss. In addition, partially to completely recrystallised igneous zircon grains have ages that define Pb-loss lines projecting towards this age. This strong evidence for a metamorphic event at ca. 2,850–2,840 Ma is confirmed by evidence for metamorphism and magmatism reported by other authors (e.g., Hokada et al. 2003). The character of the ca. 2,850 Ma metamorphic event can be constrained from observations on the relevant zircon grains. Firstly, the nature of recrystallisation and resetting of older zircon grains and fea-

tures of the zoning patterns in the metamorphic zircon (broad planar banding, embayment of oscillatory zoning) are interpreted to reflect growth during high-grade metamorphism (Corfu et al. 2003). Secondly, this event most likely occurred at pressures less than those where garnet is stable in the orthogneiss composition, as the REE patterns of ca. 2,850 Ma zircon from Dallwitz Nunatak (Fig. 4f) do not show HREE depletion characteristic of growth in the presence of garnet. Hence, we infer that the ca. 2,850 Ma metamorphic/magmatic event was of low-*P*/high-*T* type and not related to the ~8–11 kbar UHT metamorphic event in the Napier Complex. This interpretation differs from that of Harley and Black (1997), who suggested that UHT metamorphism occurred between 2,850 and 2,820 Ma.

The ca. 2,850–2,840 Ma event is the earliest tectonothermal event that can be conclusively identified within the Napier Complex, and the distribution of ages at this time (Dallwitz Nunatak, Mt Sones, Mt Riiser Larsen, Proclamation Is) indicates that this event was regionally extensive. In addition, no compelling evidence exists to suggest that the northern and central Napier Complex experienced separate early histories, as tentatively proposed by Harley and Black (1997). On the basis of our reassessment of the available evidence, the Napier Complex most likely formed a single cratonic block, from at least ca. 2,850 Ma and possibly as far back as ca. 3,000 Ma.

Zircon response to UHT metamorphism in the Napier Complex

Late Archaean-Palaeoproterozoic zircon ages are ubiquitous to all samples within this study (Table 6), with similar ages (2,480–2,500 Ma) occurring in the three orthogneiss samples. Highly luminescent grains and rims from Proclamation Island charnockite that are interpreted to reflect growth at high temperatures, probably in the presence of partial melt, have $^{207}Pb/^{206}Pb$ ages between 2,510 and 2,470 Ma (pooled age: ca. 2,490 Ma). The REE patterns of these zircon rims are not distinct to other generations in the sample, making it difficult to link this age to a particular fabric. However, in the Gage Ridge orthogneiss a generation of weakly luminescent, homogeneous or banded zircon rims that also define an age population at ca. 2,486 Ma are chemically distinct from an earlier population of visually similar rims. These ca. 2,486 Ma rims are slightly HREE-depleted and have REE patterns that approach those typical of zircon that has grown in the presence of garnet.

Weakly to moderately luminescent ca. 2,485 Ma grains from the Dallwitz Nunatak orthogneiss have distinctive MREE–HREE patterns that are also consistent with growth in the presence of garnet. S_1 orthopyroxene from this sample also displays HREE-depleted patterns that are interpreted to represent growth in a garnet-bearing (S_1) assemblage. Hence, the age of this zircon population provides a minimum estimate for the equilibration of the dominant S_1 assemblage in the Dallwitz Nunatak orthogneiss. Although this rock was originally interpreted to have intruded syn-tectonic with a "D_1" event at ca. 2,850 Ma (Harley and Black 1997), data presented above indicate that intrusion occurred at some time before ca. 2,930 Ma and that the orthogneiss was subsequently metamorphosed at ca. 2,850–2,840 Ma. Given the new zircon chemistry and U–Pb data we now infer that the dominant orthopyroxene-bearing fabric at Dallwitz Nunatak was developed along with garnet in a medium-*P* metamorphic event with a *minimum* age of ca. 2,485 Ma. This *minimum* age is comparable to that previous preferred for D_3–M_3 by some authors (e.g., Black et al. 1983b, 1986a, 1986b; Harley and Black 1997), and to the age preferred for UHT metamorphism by others (e.g., Grew 1998; Carson et al. 2002b; Hokada et al. 2003). Before going further and evaluating the relative merits of these alternative interpretations it is instructive to consider in detail the age and zircon REE chemistry data recorded in the Zircon Point paragneiss.

Whilst the orthogneiss samples record a single age, the Zircon Point paragneiss records a more complex history involving up to four generations of "metamorphic" zircon growth between ca. 2,550 and ca. 2,490 Ma. All generations of zircon have HREE-depleted patterns consistent with their growth in the presence of, or at least influenced by, garnet. As the coarse-grained garnet present in this sample is in textural equilibrium with UHT mesoperthite, the age of zircon that formed in equilibrium with this garnet will in theory provide the (minimum) age of equilibration of the UHT assemblage.

Zircon population 1 (2,543 ± 41 Ma) is MREE–HREE-enriched relative to the other metamorphic zircon in the paragneiss. This zircon is also HREE-enriched relative to typical concentrations expected for metamorphic zircon that has grown in competition with garnet (~60–200×chondrite; Bea 1996; Bea and Montero 1999; Harley et al. 2001; Rubatto 2002; Whitehouse and Platt 2003; N.M. Kelly unpublished data), for which the MREE–HREE in zircon are generally 0.7–1.0 times the concentrations observed in garnet. The high MREE–HREE concentrations suggests that whilst zircon growth occurred in the presence of garnet, which exerted a strong influence on REE budget and partitioning, the REE reservoir in the rock was not totally depleted. Therefore, the first generation of new zircon growth is interpreted to have occurred early in the reaction history prior to significant garnet growth in the paragneiss. Zircon populations 2 and 3 (2,511 ± 17 Ma and 2,490 ± 17 Ma, respectively) have MREE–HREE concentrations less than that observed in garnet and more consistent with concentrations typical for zircon grown with low-Ca garnet in a metapelite (Harley et al. 2001). Using average garnet and zircon REE concentrations from population 2, calculated zircon-garnet D_{REE} values decrease slightly from $D_{Sm} \approx 0.9$ to $D_{Gd} \approx 0.7$, before increasing slightly to 0.8 at Ho (Fig. 11). Zircon population 3 produces similar D_{REE} values ($D_{Sm} \approx 1.2$, D_{Gd}

Table 6 Age and event summary for the samples analysed during this study

Gage Ridge (o/gneiss)		Proclamation Island (o/gneiss)		Dallwitz Nunatak (o/gneiss)		Zircon Point (p/gneiss)		Inferred event
Age	Zircon type/ REE pattern	Age	Zircon type/ REE pattern	Age	Zircon type/REE pattern	Age	Zircon type/ REE pattern	
3851 ± 62 Ma *3840 ± 30/20 Ma*	Oscillatory zoned and disturbed zircon cores; steep "magmatic" REE patterns							Magmatic; restricted area now exposed
		2988 ± 23 Ma *2980 ± 9 Ma*	Oscillatory zoned grains; steep REE	**> 2933 ± 25 Ma**	Oscillatory zoned grains; steep REE			Magmatic; widespread event
2848 ± 460 Ma	upper intercept age: disturbed grains	**2854 ± 14 Ma** *2847 ± 11 Ma*	Disturbed cores, low CL zoned and homogeneous outer cores/rims; slightly MREE depleted relative to magmatic zircon	**2840 ± 20 Ma** *2850 ± 40/20 Ma*	Disturbed cores, low CL banded outer cores/rims; very steep REE: MREE-depleted & HREE enriched relative to magmatic zircon	*2822 ± 22 Ma*	Inherited, oscillatory zoned cores; steep "magmatic" REE patterns	High-grade metamorphism; below garnet-grade in intermediate orthogneiss
No zircon growth	*No zircon growth*	*No zircon growth*	**2543 ± 41 Ma**	Low-mod CL, planar banded/ sector zoned cores; depleted "flat" HREE patterns	UHT metamorphism; limited zircon growth in orthogneiss			
No zircon growth	*No zircon growth*	*No zircon growth*	**2511 ± 17 Ma (2505 ± 26 Ma)** *2508 ± 38 Ma*	Mod CL, planar banded rims; depleted "flat" HREE patterns	UHT metamorphism; limited zircon growth in orthogneiss			
2486 ± 8 Ma (95% confid.)	Planar banded/sector zoned, homogeneous cores & rims; HREE depleted relative to magmatic cores, rare flat patterns; enhanced Eu anomaly	**2487 ± 10 Ma** (95% confid.)	High CL rims; slightly MREE depleted relative to magmatic zircon, pattern similar to disturbed zircon	**2485 ± 14 Ma** *2481 ± 4 Ma*	Planar banded/sector zoned cores/rims, low CL rims; depleted "flat" HREE patterns	**2490 ± 17 Ma**	High CL, planar banded/ sector zoned outer cores/rims; depleted "flat" HREE patterns	Waning stages of UHT event? Dominant growth of zircon in orthogneiss; zircon growth from melt in orthogneiss & paragneiss

Ages in italics are taken from Harley and Black (1997)

$\approx$0.7, increasing at Ho to 0.8 and at Er to 0.9; $D_{Lu} \approx$1.1). The more pronounced increase in D_{REE} values at the heaviest end of the REE reflects a minor and increasing enrichment with increasing mass of the HREE in Population 3 zircons, compared with Populations 1 and 2.

Deciding which D_{REE} pattern reflects zircon–garnet equilibrium is somewhat problematic. In the absence of direct experimental data the only realistic approach to this at present is an empirical one, involving comparison of the D_{REE} with those measured for garnet and zircon that have crystallised in leucosomes (e.g., Harley et al. 2001; Rubatto 2002), or in a definite textural relationship (Whitehouse and Platt 2003).

The mineral assemblage preserved in the Zircon Point paragneiss reflects equilibration at UHT conditions, and internal zoning features within zircon populations 2 and 3 suggest that they grew in the presence of partial melt (Fig. 5a, e). Moreover, major minerals such as garnet are not zoned and show no evidence for post-peak reaction or retrogression. However, the zircon generations that may potentially be in equilibrium with this assemblage are not uniform in REE composition. The calculated zircon–garnet D_{REE} values obtained by using all zircon populations (1, 2 and 3) contrast greatly with those proposed by Rubatto (2002) for zircon and garnet grown from a granulite facies melt (D_{REE} increases steadily from $D_{Gd} \approx$0.94 to $D_{Lu} \approx$12.1 in Rubatto 2002; Fig. 11). The pattern reported by Rubatto (2002) was calculated using average zircon rim compositions that preserve steep REE patterns (Yb/Gd$\approx$40–67), more consistent with compositions reported in other studies for zircon grains that have grown in garnet-absent lithologies (Heamann et al. 1990; Hinton and Upton 1991; Barbey et al. 1995; Rubatto et al. 2001). The D_{REE} values reported by Rubatto (2002) are close to those calculated using the composition of detrital magmatic zircon from the Zircon Point paragneiss (Fig. 10). This steep REE pattern was explained by Rubatto (2002) to have resulted from growth in an ''open'' system, and therefore an unlimited trace element reservoir that would not be controlled by REE sequestered into garnet. If this explanation is valid, the D_{REE} reported by Rubatto (2002) will not pertain to zircon–garnet equilibrium. Alternatively, the zircon analysed may have grown from or in an earlier melt composition prior to the growth of garnet.

In contrast to the D_{REE} values proposed by Rubatto (2002) are the zircon–garnet D_{REE} values that were published by Whitehouse and Platt (2003) for zircon formed in equilibrium with the rims of zoned garnet porphyroblasts. These values ($D_{Sm} \approx$0.45, $D_{Gd} \approx$0.55, $D_{Dy\text{-}Lu} \approx$0.8, $D_{Er} \approx$1; Fig. 11) are more consistent with those calculated here for zircon and garnet compositions in the Zircon Point paragneiss, in particular those calculated from Populations 2 and 3. Moreover, their D_{REE} are similar to those calculated from UHT leucosomes from the Napier Complex by Harley et al. (2001; $D_{Sm} \approx$1–2, decreasing to $D_{Gd} \approx$0.9 and $D_{Lu} \approx$0.7).

The minor differences between zircon–garnet D_{REE} patterns for Zircon Point populations 2 and 3, which result from a minor HREE-enrichment in population 3, suggests that population 2 may be closest to an equilibrium condition with the garnet composition measured in the Zircon Point paragneiss. If this is true, the garnet-bearing UHT mineral assemblage equilibrated with zircon at $\geq$2,511 ± 17 Ma and peak UHT metamorphism must be at least this age. The texturally youngest zircon generation, weakly luminescent, high-U rims (2 dated) have $^{207}Pb/^{206}Pb$ ages that are slightly older than the highly luminescent zircon that they enclose (e.g., 2,545 ± 10 Ma rim on 2,504 ± 10 Ma highly luminescent outer core: Fig. 5e), although these ages are just within 2σ error of each other. The oldest analysis of highly luminescent zircon (Population 3) is 2,517 ± 16 Ma (n38.1; Table 5), suggesting that the younger ages within this group may be an analytical artefact or reflect partial resetting following growth at or before ca. 2,545 Ma. Consequently, an age of UHT fabric formation older than 2,545 ± 10 Ma cannot be excluded on the basis of our analyses.

Contrasting zircon ages during UHT metamorphism

All four rocks discussed in detail in this paper preserve zircon grains with ages between ca. 2,500–2,480 Ma. This is a common age reported for ''metamorphic'' zircon in the Napier Complex and is widely interpreted as the age of UHT metamorphism (Grew and Manton 1979; Grew et al. 1982; DePaolo et al. 1982; Sandiford and Wilson 1984; Grew 1998; Carson et al. 2002b; Hokada et al. 2003, 2004). However, the Zircon Point paragneiss preserves evidence for zircon growth *prior* to

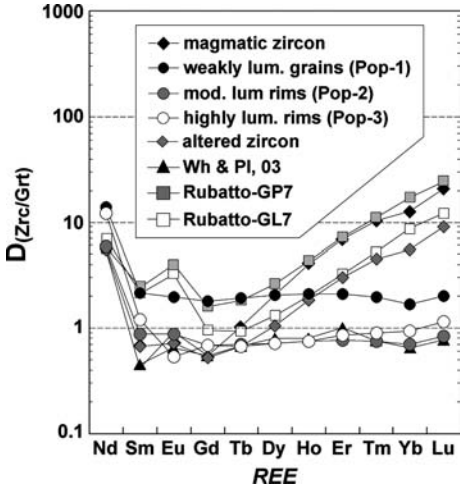

Fig. 11 Rare earth element partitioning coefficients for coexisting zircon and garnet from Zircon Point paragneiss. Selected published values are provided for comparison and are discussed in the text. D_{REE} (Zrc/Grt) = $REE_{zircon}/REE_{garnet}$ using measured values (ppm). Zircon Point values are averages of measured values for each zircon population type. Published values: Wh & Pl, 03: Whitehouse and Platt (2003); Rubatto-GP7 and -GL7: Rubatto (2002)

this time, and based on inferred equilibrium between zircon and S_1 garnet at this locality, the UHT assemblage equilibrated at some time before ca. 2,510 Ma, and perhaps before ca. 2,545 Ma. In addition, garnet-bearing leucosomes that are interpreted to cut the UHT fabric at nearby McIntyre Island contain zircon grains that equilibrated with garnet between 2,590 and 2,556 Ma (Harley et al. 2001; Harley 2002). At Tonagh Island, 2,626 ± 28 Ma orthogneiss that intruded prior to the UHT metamorphism places an upper age limit on the UHT event (Carson et al. 2002b). Although the gneisses at Tonagh Island show abundant zircon ages between 2,480 and 2,450 Ma, they also preserve an earlier phase of metamorphic zircon growth at ca. 2,545 Ma (Shiraishi et al. 1997; Carson et al. 2002b; Crowe et al. 2002). Hence there exists a major disparity (110–65 million years) between the ages that may be inferred for "peak" metamorphism during an apparently single tectonothermal event.

It is well understood that an age obtained from a particular textural zone within a zircon grain dates the timing of growth or reflects a subsequent process or processes that may have partially or completely reset this growth age. In the case of relatively un-reactive rocks such as felsic orthogneisses and quartzofeldspathic paragneisses, the growth of new zircon is largely restricted to recrystallisation or dissolution/reprecipitation of pre-existing zircon, or crystallisation from a Zr-bearing anatectic melt. The resulting zircon will therefore date the (re)crystallisation event. It is possible that the predominance of younger zircon ages in such rocks is related to volume-diffusion and/or fracture-assisted diffusion of Pb during an extended period of cooling from high temperatures (e.g., Ashwal et al. 1999). However, it would be unreasonable to expect uniform Pb-loss across the Napier Complex at a specific time, so the relatively consistent ages (ca. 2,480 Ma) observed in so many samples, including those from areas outside the UHT zone (Proclamation Island, this study) are unlikely to be explained in this manner. Moreover, in samples investigated in this study where younger ages are recorded, zircon grains are not systematically affected by extensive microfracturing. Alternatively, it is also possible that the Napier Complex was subjected to pervasive resetting during a fluid-dominated event that occurred late in the cooling history, although evidence for an event of this kind on a regional scale has yet to be found.

At high temperatures (> 900°C) zirconium saturation in a granitic melt would be such that in most rocks zircon would dissolve into a melt rather than precipitate from it (Roberts and Finger 1997). At the peak conditions inferred for the Napier Complex (> 1,000–1,100°C, ~10 kbar; Harley and Motoyoshi 2000) most felsic rocks will have undergone some degree of partial melting, and consequently zircon dissolution. In this case zircon growth would not be expected to have occurred at *peak* conditions. According to the model of Roberts and Finger (1997), in a rock of typical granitic composition (Zr≈100–200 ppm) crystallisation of new zircon would only begin between 900 and 800°C when X_{H2O} increases and Zr solubility in the melt decreases. Following peak conditions in the Napier Complex, the terrain underwent minor decompression to ~8–9 kbars (Hollis and Harley 2002) followed by an extended period of near-isobaric cooling, suggesting that a considerable time may have passed before significant zircon growth occurred. It is possible then that the bulk of zircon ages from the Napier Complex reflect the late, *post-peak* crystallisation of zircon on cooling of melts beyond their saturation Zr contents.

The minor occurrence of ca. 2,550 Ma ages (Shiraishi et al. 1997; Harley et al. 2001; Carson et al. 2002b; Crowe et al. 2002; this study), coupled with textural and chemical constraints on the possible timing of UHT metamorphism (ca. 2,550–2,590 Ma; Harley 2002; Carson et al. 2002b; this study) suggests that some zircon growth *did* occur closer to peak conditions, possibly through dissolution/reprecipitation processes or through the breakdown of a Zr-bearing phase during prograde metamorphism. The predominance of ages from the Napier Complex falling between ca. 2,500 and 2,480 Ma points towards there being a major post-peak process controlling zircon growth or isotopic resetting that is not as yet fully understood. The similarity to ages obtained from monazite in the Napier Complex (Asami et al. 1998, 2002) may be used as evidence that this resetting process operated at only 750–800°C.

Defining the age of deformation events

Based on the D_1–D_3 structural model for the Napier Complex (James and Black 1981), it is generally accepted that the D_1–D_2 events are associated with the development of UHT mineral assemblages (Grew et al. 1982; Sheraton et al. 1987; Harley and Black 1997; Grew 1998; Carson et al. 2002b; Hokada et al. 2003). Although there is now general agreement that the UHT event *did not* occur at ca. 2,850 Ma or earlier (Carson et al. 2002b; Harley et al. 2001), there is still controversy and debate over exactly when these structures, and therefore UHT mineral assemblages, developed (Grew 1998; Carson et al. 2002b; Harley 2002; Hokada et al. 2003, 2004). Moreover, it is not clear whether apparently similar structures and fabrics developed during equivalent deformation events across the entire terrain.

Further difficulties surrounding the age definition of deformation events arise from the interpretation of "syn-deformation" intrusions. For example, Black et al. (1983b) interpreted the syn-tectonic pegmatites in the Casey Bay region to be "syn-D_3", whereas Sandiford and Wilson (1984) suggested there were emplaced during D_2 boudinage at UHT conditions. The interpretation of syn-deformational orthogneisses at Dallwitz Nunatak and Proclamation Island (Sheraton et al. 1980; James and Black 1981; Black et al. 1986a; Harley and Black 1997) has been key to placing time constraints on deformation/metamorphic events in the Napier Com-

plex. However, it has been shown in other high-grade terranes that the interpretation of what constitutes an igneous or tectonic contact may be highly controversial (e.g., Akilia, SW Greenland: Nutman et al. 1997; Myers and Crowley 2000; Mojzsis and Harrison 2002; Whitehouse and Fedo 2003), and in the case of the Dallwitz Nunatak orthogneiss, it is now apparent that the syn-deformation interpretation is no longer sustainable.

The current study has demonstrated that S_1 in the Dallwitz Nunatak orthogneiss, originally interpreted to be contemporaneous with S_1 in the host orthogneiss, equilibrated with zircon at or before ca. 2,490 Ma, suggesting that the "D_1" event is actually of this age and not ca. 2,850–2,840 Ma. Moreover, zircon textures and ages indicate a protolith crystallisation age of ≥2,930 Ma followed by growth of chemically distinct metamorphic zircon at ca. 2,840 Ma. The absolute age of the foliation in the host gneiss to the Dallwitz Nunatak orthogneiss is not known, but zircon evidence suggests that what is described terrain-wide as S_1 and D_1 structures, are most likely the result of multiple overprinting events and not a single tectonothermal cycle between 2,600 and 2,450 Ma. The deposition of sediments following ca. 2,850 Ma tectonism (e.g., Zircon Point paragneiss), which were subsequently interleaved and transposed into parallelism with other layered gneisses indicates that deformation during the UHT event has effectively obscured all evidence for these earlier events in these particular locations. The difficulty in distinguishing orthogneiss bodies of different ages that intruded before and after ca. 2,850 Ma tectonism compounds difficulties in identifying possible zones of low strain during the UHT event.

Conclusions

The use of an integrated textural/chemical approach to U/Pb zircon geochronology on selected samples from the Archaean Napier Complex has enabled key magmatic and metamorphic events in its history to be clarified. Important conclusions from this study are:

1. Magmatism occurred regionally at ca. 2,990 Ma, and this also is the likely age for intrusion of the Dallwitz Nunatak orthogneiss.
2. Metamorphic growth and recrystallisation of zircon occurred at ca. 2,850–2,840 Ma in the Dallwitz Nunatak orthogneiss in the absence of garnet, leading to high U (low Th/U), LREE-depleted, and more rarely, HREE-enriched zircon rims and outer cores. This zircon is interpreted to have formed through sub-solidus growth at relatively high-*T* but below the pressures required to stabilise garnet in the orthogneiss samples.
3. Zircon growth between ca. 2,550 and 2,480 Ma occurred in the presence of anatectic melt. Orthogneiss samples mostly preserve single population ages between ca. 2,480 and 2,500 Ma whereas paragneiss records three episodes of zircon growth from ca. 2,550 to 2,480 Ma. Although Th/U ratios are variable, in the UHT-zone the zircon REE patterns reflect the influence of garnet during growth and recrystallisation of zircon.
4. REE patterns from zircon grains indicate that: (a) the S_1 foliation in the Dallwitz Nunatak orthogneiss equilibrated ≥2,490 Ma and not at ca. 2,850 Ma as previously suggested; (b) UHT minerals in Zircon Point paragneiss equilibrated with zircon at ≥2,510 Ma; (c) the absolute minimum age of peak UHT metamorphism is ca. 2,510 Ma, but it is likely to be older than ca. 2,545 Ma.
5. Disparity of ages between orthogneiss and paragneiss samples is most likely to be related to mechanisms of zircon growth with respect to *P–T* conditions and rock composition. The predominance of zircon ages at ca. 2,500–2,480 Ma should *not* be interpreted to define the age of UHT metamorphism. Instead, these ages reflect post-peak processes affecting zircon that are not yet well understood but which may be related to final crystallisation of segregated melts and release of fluids.
6. REE patterns in zircon formed during metamorphism will reflect the mechanism and environment of mineral growth or recrystallisation. In the absence of a competitor phase that strongly partitions/sequesters REE, LREE-depletion/HREE-enrichment in zircon may be related to preferential expulsion of large radii REE and concentration of smaller radii REE; the presence or concurrent growth of garnet will cause variable HREE-depletion.
7. Integrated, textural/chemical approaches to U/Pb zircon geochronology are necessary to unravel the complex histories in polydeformed/metamorphosed terrains. However, consideration of full mineral textural context of analysed zircon is required if the interpretation is to be well-founded and adequate.

Acknowledgements The authors would like to acknowledge Lance Black (Geoscience Australia) for providing the grain mounts and samples and permission to re-use previously collected data. Access to SIMS was provided through NSS support at the National Environment Research Council Ion Microprobe facility, University of Edinburgh. Other analytical costs were supported through a Royal Society grant to SLH. The authors would also like to thank Nicola Cayzer (SEM), Peter Hill (EMP), Richard Hinton and John Craven (SIMS) for analytical assistance at the School of GeoSciences, University of Edinburgh, and Mark Fanning, Research School of Earth Sciences, ANU, for assistance with SHRIMP II. NMK would like to acknowledge salary and additional support through a Royal Society of Edinburgh/SEELLD Research Fellowship. The authors would like to thank E. Grew and M. Whitehouse for careful and constructive reviews of this manuscript.

References

Anders E, Grevasse N (1989) Abundances of the elements—meteoritic and solar. Geochim Cosmochim Acta 53:197–214

Asami M, Suzuki K, Grew ES, Adachi M (1998) CHIME ages for granulites from the Napier Complex, East Antarctica. Polar Geosci 11:172–199

Asami M., Suzuki K, Grew ES (2002) Chemical Th-U-total Pb dating by electron microprobe analysis of monazite, xenotime and zircon from the Archaean Napier Complex, East Antarctica: evidence for ultra-high-temperature metamorphism at 2,400 Ma. Precambr Res 114:249–275

Ashwal LD, Tucker RD, Zinner EK (1999) Slow cooling of deep crustal granulites and Pb-loss in zircon. Geochim Cosmochim Acta 63:2839–2851

Barbey P, Alle P, Brouand M, Albarede F (1995) Rare-earth patterns in zircons from the Manaslu granite and Tibetan Slab migmatites (Himalaya): insights in the origin and evolution of a crustally-derived granite magma. Chem Geol 125:1–17

Bea F (1996) Residence of REE, Y, Th and U in granites and crustal protoliths; implications for the chemistry of crustal melts. J Petrol 37:521–552

Bea F, Montero P (1999) Behaviour of accessory phases and redistribution of Zr, REE, Y, Th, and U during metamorphism and partial melting of metapelites in the lower crust: an example from the Kinzigite Formation of Ivrea-Verbano, NW Italy. Geochim Cosmochim Acta 63:1133–1153

Bea F, Montero P, Garuti G, Zacharini F (1997) Pressure-dependence of rare earth element distribution in amphibolite- and granulite-grade garnets. A LA-ICP-MS study. Geostandards Newslett 21:253–270

Black LP (1988) Isotopic resetting of U–Pb zircon and Rb-Sr and Sm-Nd whole-rock systems in Enderby Land, Antarctica: implications for the interpretation of isotopic data from polymetamorphic and multiply deformed terrains. Precambr Res 38:355–365

Black LP, James PR (1979) Preliminary isotopic ages from Enderby Land, Antarctica. J Geol Soc Aus 26:266-267

Black LP, James PR, Harley SL (1983a) Geochronology and geological evolution of metamorphic rocks in the Field Islands area, East Antarctica. J Metamorphic Geol 1:277–303

Black LP, James PR, Harley SL (1983b) The geochronology, structure and metamorphism of early Archaean rocks at Fyfe Hills, Enderby Land, Antarctica. Precambr Res 21:197–222

Black LP, Sheraton JW, James PR (1986a) Late Archaean granites of the Napier Complex, Enderby Land, Antarctica: a comparison of Rb-Sr, Sm-Nd and U–Pb isotopic systematics in a complex terrain. Precambr Res 32:343–368

Black LP, Williams IS, Compston W (1986b) Four zircon ages from one rock: the history of a 3,930 Ma-old granulite from Mount Sones, Enderby Land, Antarctica. Contrib Mineral Petrol 94:427–437

Boger SD, Carson CJ, Fanning CM, Hergt JM, Wilson CJL, Woodhead JD (2002) Pan-African intraplate deformation in the northern Prince Charles Mountains, east Antarctica. Earth Planet Sci Lett 195:195–210

Carson CJ, Ague JJ, Grove M, Coath CD, Harrison TM (2002a) U–Pb isotopic behaviour of zircon during upper-amphibolite facies fluid infiltration in the Napier Complex, east Antarctica. Earth Planet Sci Lett 199:287–310

Carson CJ, Ague JJ, Coath CD (2002b) U–Pb geochronology from Tonagh Island, east Antarctica: implications for the timing of ultra-high temperature metamorphism of the Napier Complex. Precambr Res 116:237–263

Claoue-Long JC, Compston W, Roberts J, Fanning CM (1995) Two Carboniferous ages: a comparison of SHRIMP zircon dating with conventional zircon ages and 40Ar/39Ar analysis. Geochronology Time Scales and Global Stratigraphic Correlation, SEPM Special Publication No. 54, pp 3–21

Compston W, Williams IS, Meyer C (1984) U–Pb geochronology of zircons from Lunear Breccia 73217 using a sensitive high mass-resolution ion microprobe. J Geophys Res 89:525–534

Corfu F, Hanchar JM, Hoskin PWO, Kinny P (2003) Atlas of zircon textures. In: Hanchar JM, Hoskin PWO (eds) Reviews in mineralogy and geochemistry, vol 53. Zircon, Mineralogical Society of America, Washington, pp 469–495

Crowe WA, Osanai Y, Toyoshima T, Owada M, Tsunogae T, Hokada T. (2002). SHRIMP geochronology of a mylonite zone on Tonagh Island: characterisation of the last high-grade tectonothermal event in the Napier Complex, East Antarctica. Polar Geosci 15:17–36

Dallwitz WB (1968) Coexisting sapphirine and quartz in granulites from Enderby Land, Antarctica. Nature 219:476–477

Degeling H, Eggins S, Ellis DJ (2001) Zr budgets for metamorphic reactions, and the formation of zircon from garnet breakdown. Mineral Mag 65:749–758

DePaolo DJ, Manton WI, Grew ES, Halpern M (1982) Sm–Nd, Rb–Sr and U–Th–Pb systematics of granulite facies rocks from Fyfe Hills, Enderby Land, Antartica. Nature 298:614–618

Ellis DJ, Green DH (1985) Garnet-forming reaction in mafic granulites from Enderby Land, Antarctica—Implications for geothermometry and geobarometry. J Petrol 26:633–662

Ellis DJ, Sheraton JW, England RN, Dallwitz WB (1980) Osumulite–sapphirine–quartz granulites from Enderby Land, Antarctica—mineral assemblages and reactions. Contrib Mineral Petrol 72:123–143

Fraser G, Ellis D, Eggins S (1997) Zirconium abundance in granulite-facies minerals, with implications for zircon geochronology in high-grade rocks. Geology 25:607–610

Grew ES (1980) Sapphirine + quartz association from Archaean rocks in Enderby Land, Antarctica. Amer Mineral 65:821–836

Grew ES (1982) Osumilite in the sapphirine–quartz terrane of Enderby Land, Antarctica: implications for osumilite petrogenesis in the granulite-facies. Amer Mineral 67:762–787

Grew ES (1998) Boron and Beryllium minerals in granulite-facies pegmatites and implications of Beryllium pegmatites for the origin and evolution of the Archaean Napier Complex of East Antarctica. In: Motoyoshi Y, Shiraishi K (eds) Origin and evolution of continents. Proceedings of the international symposium ''Origin and Evolution of Continents''. National Institute of Polar Research, Tokyo, pp 74–92

Grew ES, Manton WI (1979) Archaean rocks in Antarctica: 2.5-billion-year uranium–lead ages of pegmatites in Enderby Land. Science 206:443–445

Grew ES, Manton WI, Sandiford M (1982) Geochronological studies in East Antarctica: age of pegmatites in Casey Bay, Enderby Land. Antarct J US 17:1–2

Grew ES, Suzuki K, Asami M (2001) CHIME ages of xenotime, monazite and zircon from beryllium pegmatites in the Napier Complex, Khmara Bay, Enderby Land, East Antarctica. Polar Geosci 14:99–118

Hanchar JM, Miller CF (1993) Zircon zonation patterns as revealed by cathodoluminescence and backscattered electron images: implications for interpretation of complex crustal histories. Chem Geol 110:1–13

Hanchar JM, Rudnick RL (1995) Revealing hidden structures: the application of cathodoluminescence and back-scattered electron imaging to dating zircons from lower crustal xenoliths. Lithos 36:289–303

Harley SL (1985) Garnet-orthopyroxene bearing granulites from Enderby Land, Antarctica: metamorphic pressure–temperature–time evolution of the Archaean Napier Complex. J Petrol 26:819–856

Harley SL (1998) An appraisal of peak temperatures and thermal histories in ultrahigh-temperature (UHT) crustal metamorphism: the significance of aluminous orthopyroxene. Mem Nat Inst Polar Rese, (Special Issue) 53:49–73

Harley SL (2002) Zircon-garnet REE distribution patterns and the behaviour of zircon during UHT metamorphism. In: International mineralogical association meeting, Edinburgh, abstract, p 236, September

Harley SL, Black LP (1997) A revised Archaean chronology for the Napier Complex, Enderby Land, from SHRIMP ion-microprobe studies. Antarctic Sci 9:74–91

Harley SL, Hensen BJ (1990) Archaean and Proterozoic high grade terranes of East Antarctica (40–80°E): a case study of diversity in granulite facies metamorphism. In: Ashworth JR Brown M (eds) High temperature metamorphism and crustal anatexis. Unwin Hyman, London, pp 320–370

Harley SL, Motoyoshi Y (2000) Al zoning in orthopyroxene in a sapphirine quartzite: evidence for >1,120°C UHT metamorphism in the Napier Complex, Antarctica, and implications for the entropy of sapphirine. Contrib Mineral Petrol 138:293–307

Harley SL, Kinny PD, Snape I, Black LP (2001) Zircon chemistry and the definition of events in Archaean granulite terrains. In: Fourth International Archaean Symposium, Extended Abstract Volume, AGSO Geoscience Australia Record 2001/37, pp 511–513

Hawkins DP, Bowring SA (1999) U–Pb monazite, xenotime and titanite geochronological constraints on the prograde to post-peak metamorphic thermal history of Palaeoproterozoic migmatites from the Grand Canyon, Arizona. Contrib Mineral Petrol 134:150–169

Heaman LM, Bowins R, Crocket J (1990) The chemical composition of igneous zircon suites: implications for geochemical tracer studies. Geochim Cosmochim Acta 54:1597–1607

Hensen BJ, Motoyoshi Y (1992) Osumilite-producing reactions in high-temperature granulites from the Napier Complex, East Antarctica: tectonic implications. In: Yoshida Y, Kaminuma K, Shiraishi K. (eds) Recent progress in Antarctic Earth Science. Terra Scientifica Publishing Company, Tokyo, pp 87–92

Hermann J, Rubatto D, Korsakov A, Shatsky VS (2001) Multiple zircon growth during fast exhumation of diamondiferous, deeply subducted continental crust (Kokchetav Massif, Kazakhstan). Contrib Mineral Petrol 141:66–82

Hinton RW, Upton BGJ (1991) The chemistry of zircon: variations within and between large crystals from syenite and alkali basalt xenoliths. Geochim Cosmochim Acta 55:3287–3302

Hokada T, Osanai Y, Toyoshima T, Owada M, Tsunogae T, Crowe WA (1999) Petrology and metamorphism of sapphirine-bearing aluminous gneisses from Tonagh Island in the Napier Complex, east Antarctica. Polar Geosci 12:49–72

Hokada T, Misawa K, Shiraishi K, Suzuki S (2003) Mid to late Archaean (3.3–2.5 Ga) tonalitic crustal formation and high-grade metamorphism at Mt Riiser-Larsen, Napier Complex, east Antarctica. Precambr Res 127:215–228

Hokada T, Misawa K, Yokoyama K, Shiraishi K, Yamaguchi A (2004) SHRIMP and electron microprobe chronology of UHT mtamorphism in the Napier Complex, east Antarctica: implications for zircon growth at >1,000°C

Hollis JA, Harley SL (2002) New evidence for the peak temperatures and the near-peak pressure-temperature evolution of the Napier Complex. In: Gamble JA, Skinner DNB, Henrys S (eds) Proceedings of the 8th International Symposium on Antarctic Earth Sciences, The Royal Society of New Zealand, Wellington, pp 19–30

Hoskin PWO, Black LP (2000) Metamorphic zircon formation by solid-state recrystallisation of protolith igneous zircon. J Metamorphic Geol 18:423–439

Hoskin PWO, Ireland TR (2000) Rare earth element chemistry of zircon and its use as a provenance indicator. Geology 28:627–630

James PR, Black LP (1981) A review of the structural evolution and geochronology of the Archaean Napier Complex of Enderby Land, Australian Antarctic Territory. Geol Soci Austr Special Publication 7:71–83

Kelly NM, Clarke GL, Carson CJ, White RW (2000) Thrusting in the lower crust: evidence from the Oygarden Islands, Kemp Land, East Antarctica. Geol Mag 137:219–234

Kelly NM, Clarke GL, Fanning CM (2002) A two-stage evolution of the Neoproterozoic Rayner Structural Episode: new U–Pb SHRIMP constraints from the Oygarden Group, Kemp Land, East Antarctica. Precambr Res 116:301–330

Ludwig KR (1999) User's manual for Isoplot/Ex, v2.3, a geochronological toolkit for Microsoft Excel. Berkeley Geochronological Centre Special Publication No. 1a, p 52

Ludwig KR (2001) Squid v1.02—a user's manual. Berkeley Geochronological Centre Special Publication No. 2, p 19

McCulloch MT, Black LP (1984) Sm-Nd isotopic systematics of Enderby Land granulites and evidence for the redistribution of Sm and Nd during metamorphism. Earth Planet Sci Lett 71:46-58

McLaren AC, Fitzgerald JD, Wlliams IS (1994) The microstructure of zircon and its influence on the age determination from Pb/U isotopic ratios measured by ion microprobe. Geochim Cosmochim Acta 58:993–1005

Mezger K, Krogstad J (1997) Interpretation of discordant U–Pb zircon ages: an evaluation. J Metamorphic Geol 15:127–140

Mojzsis SJ, Harrison TM (2002) Establishment of a 3.83 Ga magmatic age for the Akilia tonalite (southern West Greenland). Earth Planet Sci Lett 202:563–576

Motoyoshi Y, Hensen BJ (1989) Sapphirine–quartz–orthopyroxene symplectites after cordierite in the Archaean Napier Complex, Antarctica: evidence for a counterclockwise *P–T* path? Eur J Mineral 1:467–471

Murali AV, Parthasarathy R, Mahadevan TM, Sankar Das M (1983) Trace element characteristics, REE patterns and partition coefficients of zircons from different geological environments—a case study on Indian zircons. Geochim Cosmochim Acta 47:2047–2052

Myers JS, Crowley JL (2000) Vestiges of life in the oldest Greenland rocks? A review of early Archaean geology in the Godthabsfjord region, and reappraisal of field evidence for >3,850 Ma life on Akilia. Precambr Res 103:101–124

Nutman AP, Mojzsis SJ, Friend CRL (1997) Recognition of ≥3,850 Ma water-lain sediments in West Greenland and their significance for the early Archaean Earth. Geochim Cosmochim Acta 61:2475–2484

Osanai Y, Toyoshima T, Owada M, Tsunogae T, Hokada T, Crowe WA (1999) Geology of ultrahigh-temperature metamorphic rocks from Tonagh Island in the Napier Complex, East Antarctica. Polar Geosci 12:1–28

Paces JB, Miller JD (1993) Precise U–Pb ages of Duluth Complex and related mafic intrusions, Northeastern Minnesota: geochronological insights into physical, petrogenetic, palaeomagnetic, and tectonomagnetic processes associated with the 1.1 Ga midcontinental rift system. J Geophys Res 98:13997–14013

Pan Y (1997) Zircon- and monazite-forming metamorphic reactions at Manitouwadge, Ontario. Can Mineral 35:105–118

Pupin JP (1980) Zircon and granite petrology. Contrib Mineral Petrol 73:207–220

Roberts MP, Finger F (1997) Do U–Pb zircon ages from granulites reflect peak metamorphic conditions? Geology 25:319–322

Rubatto D (2002) Zircon trace element geochemistry: partitioning with garnet and the link between U–Pb ages and metamorphism. Chem Geol 184:123–138

Rubatto D, Gebauer D (2000) Use of cathodoluminescence for U–Pb zircon dating by ion microprobe: some examples from the Western Alps. In: Pagel M, Barbin V, Blanc P, Ohnenstetter D (eds) Cathodoluminescence in geosciences. Springer, Berlin Heidelberg New York, pp 373–400

Rubatto D, Gebauer D, Fanning M (1998) Jurassic formation and Eocene subduction of the Zermatt-Saas-Fee ophiolites: implications for the geodynamic evolution of the Central and Western Alps. Contrib Mineral Petrol 132:269–287

Rubatto D, Williams IS, Buick IS (2001) Zircon and monazite response to prograde metamorphism in the Reynolds Range, central Australia. Contrib Mineral Petrol 140:458–468

Sandiford M (1985) The origin of retrograde shear zones in the Napier Complex: implications for the tectonic evolution of Enderby Land, Antarctica. J Struct Geol 7:477–488

Sandiford M, Wilson CJL (1984) The structural evolution of the Fyfe Hills-Khmara Bay region, Enderby Land, east Antarctica. Aust J Earth Sci 31:403–426

Schaltegger U, Fanning CM, Gunther D, Maurin JC, Schulmann K, Gebauer D (1999) Growth, annealing and recrystallisation of zircon and preservation of monazite in high-grade metamorphism: conventional and in-situ U–Pb isotope, cathodoluminescence and microchemical evidence. Contrib Mineral Petrol 134:186–201

Sheraton JW, Black LP (1983) Geochemistry of Precambrian gneisses: relevance for the evolution of the East Antarctic Shield. Lithos 16:273–296

Sheraton JW, Offe LA, Tingey RJ, Ellis DJ (1980) Enderby Land, Antarctica—an unusual Precambrian high-grade metamorphic terrain. J Geol Soci Austr 27:1–18

Sheraton JW, Tingey RJ, Black LP, Offe LA, Ellis DJ (1987) Geology of an unusual Precambrian high-grade metamorphic terrane—Enderby Land and western Kemp Land, Antarctica. Australian Bureau of Mineral Resources Bulletin 223, p 51

Shiraishi K, Ellis DJ, Fanning CM, Hiroi Y, Kagami H, Motoyoshi Y (1997) Re-examination of the metamorphic and protolith ages if the Rayner Complex, Antarctica: evidence for the Cambrian (Pan-African) regional metamorphic event. In: Ricci CA (ed) The Antarctic region: geological evolution and processes. Terra Antarctica Publication, Siena, pp 79–88

Suzuki S (2000) Geochemistry and geochronology of ultra-high temperature metamorphic rocks from the Mount Riiser-Larsen area in the Archaean Napier Complex, East Antarctica. Unpub. PhD thesis, The Graduate University for Advanced Studies, Tokyo

Vavra G (1990) On the kinematics of zircon growth and its petrogenetic significance: a cathodoluminescence study. Contrib Mineral Petrol 106:90–99

Vavra G (1994) Systematics of internal zircon morphology in major Variscan granitoid types. Contrib Mineral Petrol 117:331–344

Vavra G, Gebauer D, Schmid R, Compston W (1996) Multiple zircon growth and recrystallisation during polyphase Late Carboniferous to Triassic metamorphism in granulites of Ivrea Zone (Southern Alps): an ion microprobe (SHRIMP) study. Contrib Mineral Petrol 122:337–358

Watson EB, Liang Y (1995) A simple model for sector zoning in slowly grown crystals: implications for growth rate and lattice diffusion, with emphasis on accessory minerals in crustal rocks. Amer Mineral 80:1179–1187

Whitehouse MJ, Fedo CM (2003) Deformation features and critical field relationships of early Archaean rocks, Akilia, southwest Greenland. Precambr Res 126:259–271

Whitehouse MJ, Kamber BS (2002) On the overabundance of light rare earth elements in terrestrial zircons and its implication for Earth's earliest magmatic differentiation. Earth Planet Sci Lett 204:333–346

Whitehouse MJ, Kamber BS (2003) A rare earth element study of complex zircons from early Archaean Amitsoq gneisses, Godthabsfjord, south-west Greenland. Precambr Res 126:363–377

Whitehouse MJ, Platt JP (2003) Dating high-grade metamorphism—constraints from rare-earth elements in zircon and garnet. Contrib Mineral Petrol 145:61–74

Wiedenbeck M (1995) An example of reverse discordance during ion microprobe zircon dating: an artifact of enhanced ion yields from a radiogenic labile Pb. Chem Geol 125:197–218

Williams IS (1998) U–Th–Pb geochronology by ion microprobe. Rev Econ Geol 7:1–35

Williams IS, Compston W, Black LP, Ireland TR, Foster JJ (1984) Unsupported radiogenic Pb in zircon: a cause of anomalously high Pb–Pb, U–Pb, and Th–Pb ages. Contrib Mineral Petrol 88:322–327